The latency of a visual evoked potential tracks the onset of decision making

Michael D. Nunez[1,2,*], Aishwarya Gosai[2,3], Joachim Vandekerckhove[2,4,5], Ramesh Srinivasan[1,2,5]

[1]*Department of Biomedical Engineering, University of California, Irvine, CA, USA*
[2]*Department of Cognitive Sciences, University of California, Irvine, CA, USA*
[3]*Massachusetts General Hospital and Harvard Medical School, Boston, MA, USA*
[4]*Department of Statistics, University of California, Irvine, CA, USA*
[5]*Institute of Mathematical Behavioral Sciences, University of California, Irvine, CA, USA*

Running title: Visual evoked potentials track decision onset

[*]**Corresponding Author:**
Michael D. Nunez, PhD
Department of Biomedical Engineering
Henry Samueli School of Engineering
University of California, Irvine
Irvine, CA 92697
USA
Email: **mdnunez1@uci.edu**

Number of pages: 47

Number of figures: 9

Number of tables: 2

Number of words in Abstract: 221

Number of words in Introduction: 633

Number of words in Discussion: 1490

Conflict of interest statement: The authors declare no competing financial interests.

Acknowledgements: MDN, JV, and RS were supported by NSF grant #1658303. AG was supported by the Summer Undergraduate Research Program at the University of California, Irvine. Siyi Deng and Sam Thorpe are thanked for their contributions to the FEM solutions and anatomical fMRI image generation. Gabriel Weindel is thanked for his early comments and reanalysis of the public data paired with this paper. We would also like to thank Paul L. Nunez for his comments on the spline-Laplacian-localization technique used in this paper. This study extends initial work presented in Chapter 4 of the PhD dissertation by Nunez (2017).

Author Contributions: MDN, JV, and RS designed research. AG and MDN performed research. MDN analyzed data. MDN, AG, JV, and RS wrote the paper.

Abstract

Encoding of a sensory stimulus is believed to be the first step in perceptual decision making. Previous research has shown that electrical signals recorded from the human brain track evidence accumulation during perceptual decision making (Gold and Shadlen, 2007; O'Connell et al., 2012; Philiastides et al., 2014). In this study we directly tested the hypothesis that the latency of the N200 recorded by EEG (a negative peak occurring between 150 and 275 ms after stimulus presentation in human subjects) reflects the visual encoding time (VET) required for completion of figure-ground segregation before evidence accumulation. Simulations of cognitive decision-making theory show that variation in human response times not related to evidence accumulation (including VET) are tracked by the fastest response times. A one-to-one relationship between N200 latencies and VET was found by directly fitting a linear model between trial-averaged N200 latencies and the 10th percentiles of response times. A one-to-one relationship was also found between single-trial N200 latencies and response times. Fitting a novel neuro-cognitive model of decision-making also showed a 1-to-1 relationship between N200 latency and non-decision time, indicating that N200 latencies track the completion of visual encoding and the onset of evidence accumulation. The N200 waveforms were localized to the cortical surface at temporal and extrastriate locations, consistent with a distributed network engaged in figure-ground segregation of the target stimulus.

Key words: decision making; figure-ground segregation; EEG; visual evoked potentials (VEP), diffusion models; hierarchical Bayesian methods

Significance Statement

Encoding of a sensory stimulus is believed to be the first step in perceptual decision making. In this study, we report evidence that visual evoked potentials (EPs) around 200 ms after stimulus presentation track the time of visual figure-ground segregation before the onset of evidence accumulation during decision making. These EP latencies vary across individuals, are modulated by external visual noise, and have a one-to-one relationship with response time. Hierarchical Bayesian model-fitting was also used to relate these EPs to a specific cognitive parameter that tracks time related to visual encoding in a decision-making model of response time. This work adds to the growing literature that suggests that EEG signals can track the component cognitive processes of decision making.

Introduction

We define *visual encoding time* (VET) as the amount of time for visual processing to occur in the human brain before decision processes can begin. While there has been abundant evidence of visual information appearing in the primary visual cortex approximately 60 milliseconds (ms) after stimulus onset (Schmolesky et al., 1998; Luck, 2012), further processing takes place within a network of brain areas comprising the visual system. The key objective of this further processing is the grouping together of elements of the scene coded in separate neurons into distinct objects, a process known as figure-ground segregation (Lamme, 1995). Masking, by presenting a distractor stimulus soon after the target stimulus onset, can interrupt figure-ground segregation up to 100 ms by degrading the encoding of the visual stimulus (Lamme et al., 2002), suggesting a 160 ms VET (100 ms masking time plus 60 ms for the time of the distractor stimulus to reach primary visual cortex). Furthermore, on the basis of ERP studies in humans and physiological studies in animal models (Bach and Meigen, 1992; Roitman and Shadlen, 2002; Straube et al., 2010), VET is expected to be 150 to 200 ms in duration. Our goals in the following study were to 1) clarify estimation of VET in human subjects using EEG and 2) verify these time estimates in the framework of cognitive theory of quick human decision-making.

Human response times (time between stimulus onset and motor action execution) in decision making is theorized to be composed of VET, evidence accumulation time, response preparation time, and motor execution time. VET is separate from the decision-related processing, which has been experimentally found to reflect a sequential accumulation of evidence on level of the neuron (Gold and Shadlen, 2007; Shadlen and Kiani, 2013), the level of the scalp-recorded electroencephalograph (EEG; O'Connell et al., 2012; Philiastides et al., 2014), and on the cognitive level as evidenced by cognitive models of human behavior (Voss et al., 2004; Ratcliff and McKoon, 2008). While evidence accumulation and motor planning may operate in parallel (Dmochowski and Norcia, 2015; Servant et al., 2015, 2016), it can be reasonably expected that figure-ground segregation must occur before any evidence accumulation or motor planning in a sequential processing step. That is, the grouping of neural activity elicited by the stimulus across the visual system into a distinct "object" through figure-ground segregation is necessary before evidence accumulation and motor planning.

The figure-ground segregation speed of the human visual system has previously been estimated between 150 ms and

225 ms in humans with time-locked event related potentials (ERPs; Bach and Meigen, 1992; Thorpe et al., 1996) using clever differences between experimental conditions. Loughnane et al. (2016) found initial evidence by looking at condition differences to suggest that stimulus-locked negative peaks around 200 ms (N200) influence the onset of a neural correlate of evidence accumulation. In other studies, single-trial EEG potentials thought to be generative of N200 peaks were suspected to be related to a "pre-attentive" phase before evidence accumulation (Zhang et al., 2016, 2018). Interestingly, single-neuron recordings of evidence accumulation from lateral intraparietal areas (LIP) in primates typically begin at similar time periods after an experimental stimulus is displayed (Roitman and Shadlen, 2002; Shadlen and Kiani, 2013).

In this study, our hypothesis was that N200 peak-latencies would track VET no matter the external visual noise condition, subject, or subject's internal state that changed across EEG sessions. Using both direct linear regressions between EEG latency and fast response times and novel neuro-cognitive models of decision making, we verified that N200 peak-latencies tracked visual encoding time (VET) with a 1-to-1 correspondence at the millisecond time scale. These findings refine theory of human perceptual decision-making by finding evidence for the existence of a neural measure of the completion of figure-ground segregation and onset of evidence accumulation in the decision process.

Materials and Methods

Experiments and Participants

In order to evaluate the hypothesis that N200 latencies track VET, data was analyzed from two similar experiments. Data from Experiment 1 consisted of EEG recordings and behavioral observations from 12 unique subjects (3 female, 9 male) with 2 sessions each. Data from Experiment 2 consisted of EEG recordings and behavioral observations from 4 unique subjects (2 female, 2 male) with 7 sessions each. Two male subjects participated in both experiments resulting in 14 unique subjects across both experiments (5 female, 9 male) with 52 unique EEG sessions. Sessions of EEG collection and task performance for each subject in Experiment 1 were separated by at least 24 hours. Sessions of EEG collection and task performance for each subject in Experiment 2 were separated by 1 week. All subjects had normal or corrected-to-normal vision and had no history or family history of epilepsy. All subjects gave written

informed consent, and all data was collected at the University of California, Irvine with approval by the Institutional Review Board.

Experimental tasks

Subjects performed two-alternative forced choice tasks, specifically to determine whether a Gabor stimulus contained high or low spatial frequency content. Stimuli for Experiments 1 and 2 are built and displayed using the MATLAB Psychophysics toolbox (Psychtoolbox-3; www.psychtoolbox.org). Example stimuli are given in **Figure 1**).

Subjects performed perceptual decision making tasks in a dark room on a 61 cm LED monitor maintaining a distance of approximately 57 cm from retina to display. The monitor resolution was set as $1920 * 1280$ pixels with a 120 Hz refresh rate. The subjects were told to remain fixated on a small fixation spot while performing the task.

Gabors are sinusoidal grating patterns with a Gaussian falloff of contrast that produces maximal firing in certain neurons within the primary visual cortex (Webster et al., 1985). Subjects in both experiments were tasked with identifying the spatial frequency (either “high" or “low" spatial frequency) of large Gabors (approximately 10 cm and 10 degrees visual angle in diameter) that were randomly rotated and had a random phase on each trial (uniformly distributed draws across both rotation and phase). In Experiment 2, the high and low spatial frequencies of the target Gabors were 2.4 and 2.6 cycles per degree visual angle (cpd) respectively, while in Experiment 1, the targets were randomly drawn from a $\mathscr{B}eta(13.5, 1.5)$ distribution or a $\mathscr{B}eta(1.5, 13.5)$ distribution with means 2.4 and 2.6 cpd respectively. Both experiments contained three conditions of high, medium, and low visual noise contrast. That is, throughout each trial, samples of visual noise were displayed both before, and concurrent with the targets. In Experiment 1, a checkerboard noise pattern was displayed, while in Experiment 2, the noise was spatially bandpass filtered to include only masking noise centered around 2 and 3 cpd (i.e. the noise was a mixture of two normal distributions centered at 2 and 3 cpd with .1 cpd standard deviations), equally masking both the high and low spatial frequency targets.

The time course of each trial was as follows: subjects were asked to fixate on a small fixation spot in the center

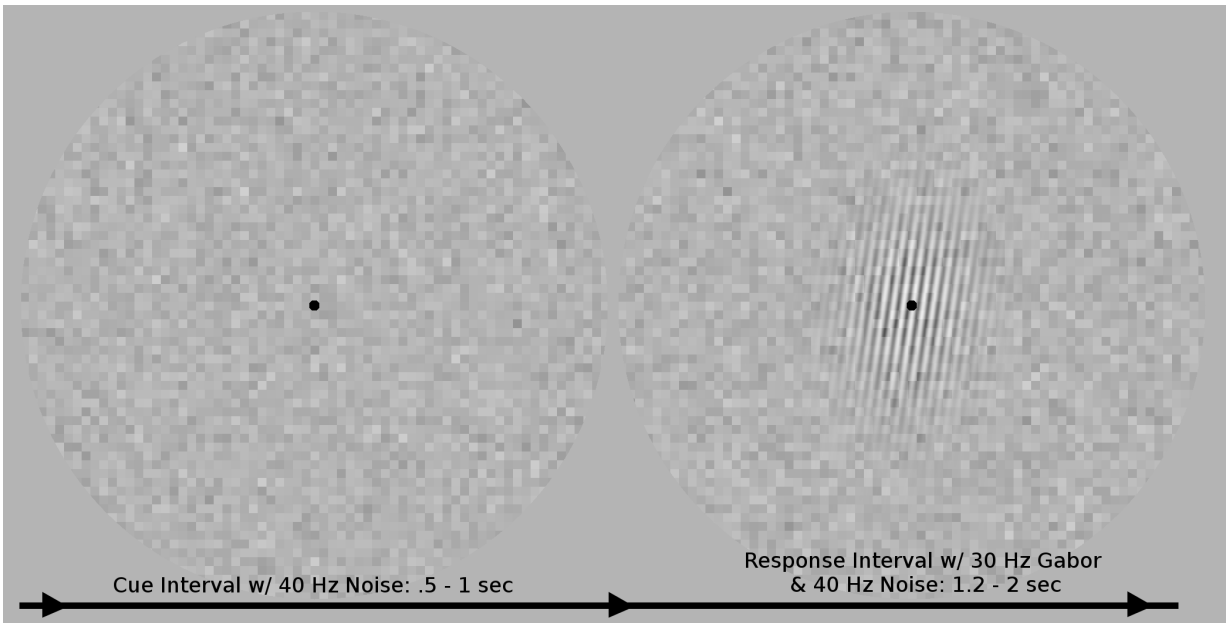

(a) Experiment 1

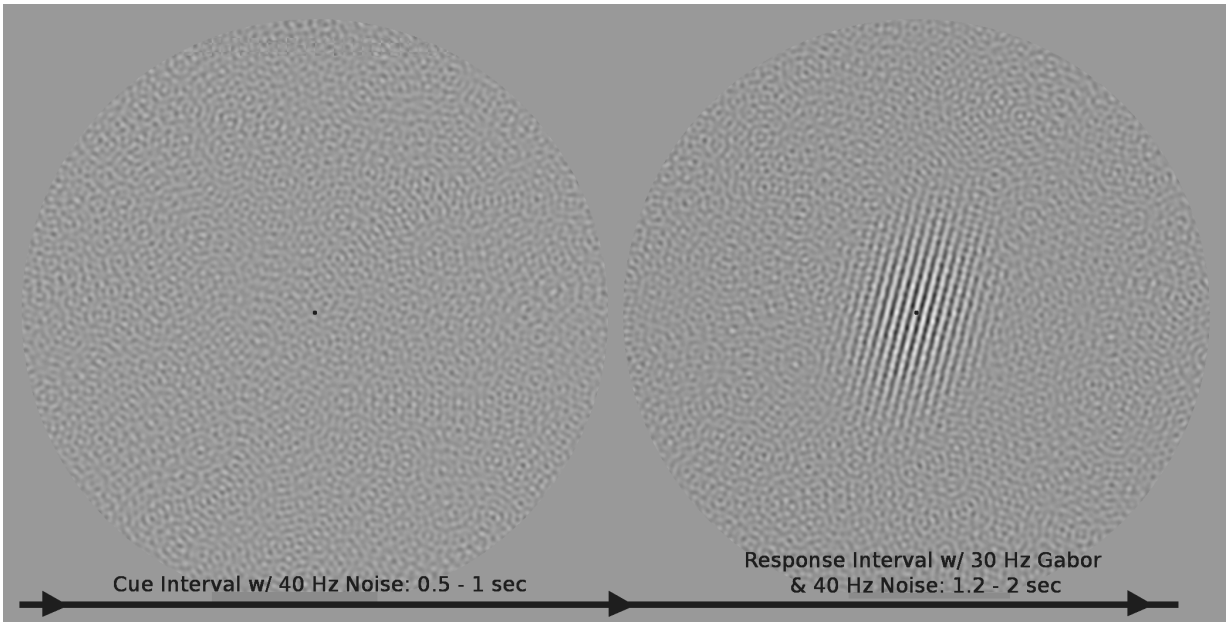

(b) Experiment 2

Figure 1. Example stimuli of the *cue* and *response* intervals of medium noise conditions from Experiments 1 (top) and 2 (bottom). During the response interval, subjects decided which spatial-frequency-target each Gabor represented, pressing a button with their left hand for a low spatial frequency target (2.4 cycles per degree visual angle, cpd) and pressing a button with their right hand for a high spatial frequency target (2.6 cpd). N200 waveforms were calculated time-locked to the onset of the Gabor stimulus during the response intervals. In both experiments a paradigm was used in which the visual noise changed at 40 Hz and the Gabor signal flickered at 30 Hz to evoke 40 Hz and 30 Hz responses in electrocortical activity that track attention to the noise and signal stimuli. While the attention analysis is not discussed in this paper, a similar analysis is presented by Nunez et al. (2015).

of the screen throughout the experiment, visual noise changing at 40 Hz was displayed a variable length of time between 500 ms to 1000 ms during the *cue* interval, then the Gabor signal stimulus was flickered at 30 Hz embedded in the noise stimuli for 1200 ms to 2000 ms during the *response* interval. During the response interval, subjects are asked to respond as accurate as possible in the time allowed using a button box, using their left hand to respond for low spatial frequency targets and their right hand for high spatial frequency targets. Auditory feedback was given after the response interval indicating trial accuracy, which was included in order to encourage subject vigilance. An entire session of task performance and EEG collection took subjects approximately 1 hour with breaks. Each session produced 8 blocks of 60 trials each for a total of 480 trials, with trials at the three levels of noise contrast intermixed within each block.

EEG recording

EEG was collected using Electrical Geodesic, Inc.'s 128 channel Geodesic sensor net and a Net Amps 200 series amplifier. Electrical activity from the scalp was recorded at a sampling rate of 1000 samples per second with a vertex reference and hardware bandpass filtered to either 1 to 50 Hz (EEG data from Experiment 1) or 1 to 100 Hz (EEG data from Experiment 2). The hardware band pass filter in Experiment 2 was chosen purposely to maintain high frequencies so that broadband noise was submitted to an Independent Component Analysis (ICA) in order to aid artifact correction. In data from both experiments, visual inspection of the raw time series and resulting ICA components was used to remove obvious artifact due to ocular movements, electrical artifact, electrode movement artifact, and some muscle (EMG) activity (see Makeig et al., 1996; Nunez et al., 2016, for further details), using the MATLAB repository artscreenEEG (Nunez et al., 2017). Both data sets ultimately yielded artifact-resistant EEG data by first removing artifactual time segments and then removing some linear electrode mixtures given by artifactual Independent Components. This artifact-resistant EEG data was common-averaged referenced then submitted to further processing as discussed below.

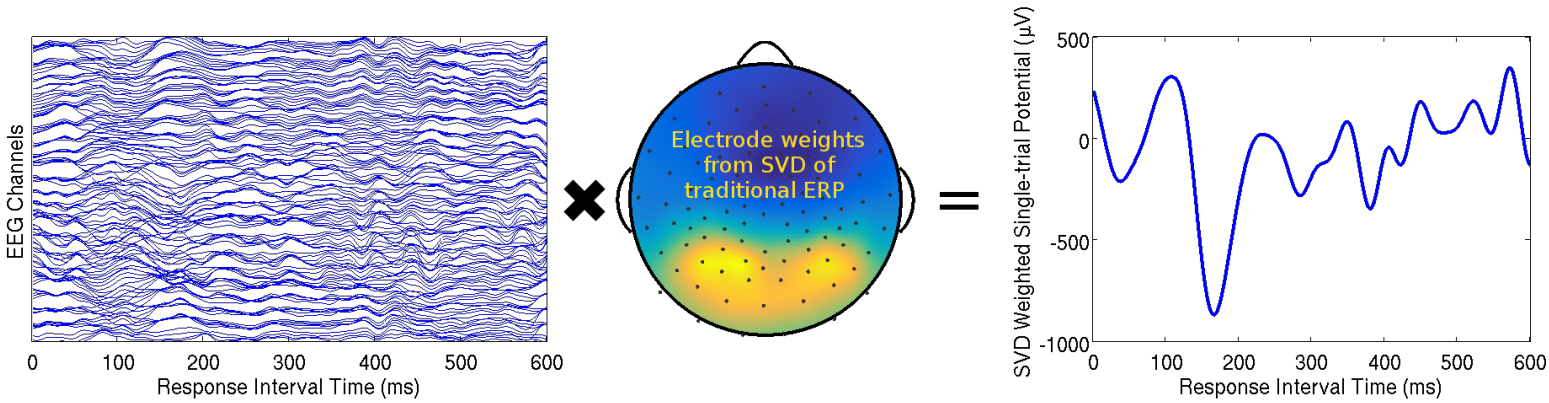

Figure 2. A visual representation of the singular value decomposition (SVD) method for finding single-trial estimates of evoked responses in EEG. The EEG presented here is time-locked to the signal onset during the response interval, such that the single-trial N200 waveform encoded the response to the signal onset. A single trial of EEG from one subject (Left) can be thought of as a time by channel ($T \times C$) matrix. SVD weights $\mathbf{v}$ ($C \times 1$) are obtained from the ERP response (i.e. trial-averaged EEG; $T \times C$) and can be plotted on a cartoon representation of the human scalp with intermediate interpolated values (Middle). This specific trial's N200 waveform (Right) was obtained by multiplying the time series data from each channel on this trial by the associated weight in vector $\mathbf{v}$ and then summing across all weighted channels. Weight averaging across channels is a common method to obtain larger signal-to-noise ratios in EEG (e.g. cleaner, more task-relevant neural signals, see Parra et al., 2005).

Estimation of N200 waveforms

N200 waveforms, calculated from the EEG signals following the onset of the Gabor patch during the *response* interval were obtained using five processing steps: 1) software bandpass filtering the EEG data to 1 to 10 Hz (forward-backward Butterowrth IIR filter with stopbands at 0.25 and 20 Hz with 1 dB attenuation in the passband and 10 dB attenuation in the stopband) obtaining cleaner estimates of evoked potentials, 2) subtracting the average baseline potential (i.e. the average amplitude in a 100 ms window before the stimulus), 3) averaging across trials to obtain a traditional ERP estimate at 128 electrodes for each subject (excluding those electrodes marked as artifact), 4) taking a singular value decomposition (SVD) of the ERPs for each experimental condition and EEG session, and then 5) using the first component (the component that explained the most variance) as an channel weighting function in order to obtain a less-noisy estimate of the N200 waveforms for each experimental condition and EEG session and for single-trial estimates (discussed below).

The goal of the singular value decomposition (SVD) was to improve the signal-to-noise ratio of both traditional ERP estimates and single-trial estimates by estimating an optimal spatial filter to detect the N200 (Kayser and Tenke, 2003; Parra et al., 2005). SVD is the algorithm used by most principal component analysis (PCA) algorithms and produces non-stochastic, deterministic results. N200 waveforms were obtained by finding the first principal component of the matrix of ERPs of 1000 ms post-stimulus and 100 ms pre-stimulus (samples T by channel C data, see Methods in Nunez et al., 2017). The first principal component consists of both a weight vector that produces a time series of the trial-average ERP and an associated vector of channel weights representing the spatial distribution of that component. Single-trial estimates of that ERP are then obtained by applying the weight vector as a spatial filter (i.e. weight summing over the vector of weights as show by **Figure 2**). It should be noted that the *first* component of the SVD method only pulled out the N200 waveform because 1) the neural response to the visual stimulus was large in the average ERP and 2) other waveform components of the ERP (such as the P300 response) were small. Had the experimental conditions been different, the N200 waveform may have been placed in a SVD component that explained less of the variance. Traditionally calculated ERPs (Luck, 2012) at specific parietal electrodes were also compared to the SVD estimated ERP and exhibited no difference in latency.

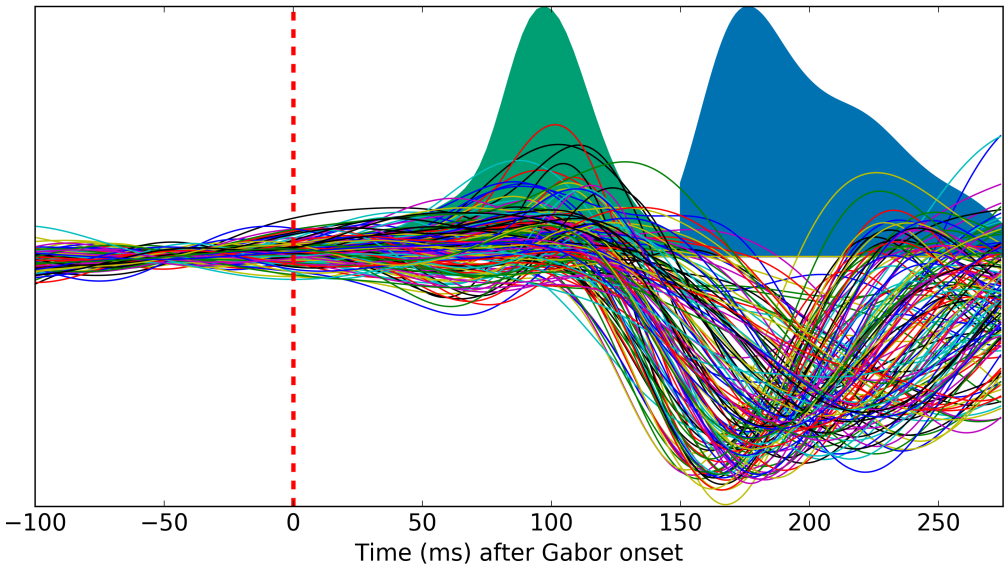

Figure 3. All trial-averaged N200 waveforms across EEG sessions and the six visual noise experimental conditions ($N = 147$). Smoothed histograms for the N200 deflection times (green distribution) as well as the N200 peak-latency times (blue distribution) are also displayed above. There was a significant but weak correlation found between the found N200 deflection times and the N200 peak-latency times ($\rho = .274$). N200 deflection times are not as variable across EEG sessions and noise conditions as N200 peak-latencies.

The window to calculate minima in order to evaluate N200 peak-latency responses was found empirically. Out of the following windows: 100 to 300 ms post-stimulus, 100 to 250 ms post-stimulus, 150 to 225 ms post-stimulus, and 150 to 275 ms post-stimulus, the 150 to 275 ms window post-stimulus was found to capture the N200 waveform on the subject-level in each condition because only 3 estimates out of 147 estimates of trial-averaged N200 peak-latency were detected at the boundary. Single-trial N200 peak-latencies that were found with a minimum on the boundary were removed from the analysis. A minimum at either 150 or 275 ms was indicative that N200 latencies were not well estimated in that noise condition or on that trial.

Deflection times were also calculated for the trial-averaged N200 waveforms by taking the window of 0 to 275 ms post-stimulus onset in the response interval and finding were the derivative of the ERP in that window first became negative before the N200 peak-latency. This reflects the point at which the signal begins to decrease before the N200 peak-latency. This particular time point has been explored in a previous study of visual encoding by Martin et al. (2010), albeit calculated using the point at which the signal reached two standard deviations below the baseline. Trial-averaged N200 waveforms and deflection time and peak-latency distributions are shown in **Figure 3**. The averaged scalp topography of these waveforms is given in the top portion of **Figure 4**.

Location of the N200 waveforms

While EEG localization is an inexact process that is unsolvable without additional assumptions, the surface spline-Laplacian (i.e. Current Source Density, CSD) has been shown to match closely to simulated cortical activity using forward models (i.e the mapping of cortical activity to scalp potentials), are unaffected by reference electrode choices, and have shown consistent results when used with real EEG data (Nunez and Srinivasan, 2006; Kayser and Tenke, 2015). In addition, unlike 3D solutions, projections to the dura mater surface with CSD are theoretically solvable, and have been used with success in past studies (see Nunez et al., 1994, for an example). Scalp topographic maps of the surface spline-Laplacian projection of the average N200 waveform across EEG sessions and noise conditions are show in the Middle panel of **Figure 4**.

Repeating a similar "source-localization" technique found in Nunez et al. (2017), we localized the curved 2D surface

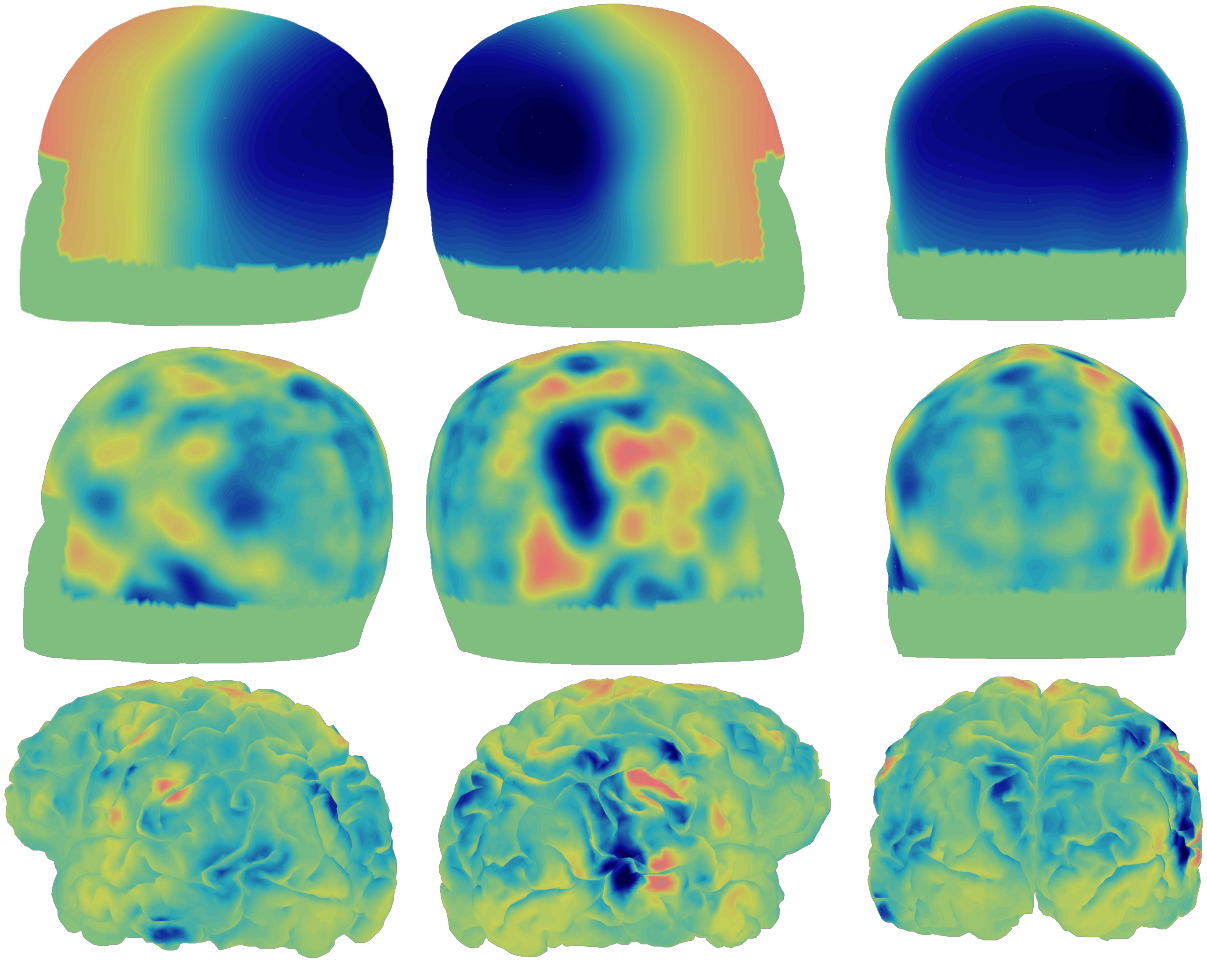

Figure 4. Left and right sagittal and posterior views of localized trial-averaged N200 waveforms averaged across all EEG recordings and noise conditions ($N = 147$). (Top) MNI scalp potential topographies (averaged projections of the first SVD components at the N200 peak-latency) were generated using spline-interpolation between electrodes. (Middle) Current Source Density MNI scalp topographies were generated with a Laplacian transform of the aforementioned data (Nunez and Pilgreen, 1991; Deng et al., 2012; Kayser and Tenke, 2015). (Bottom) The cortical maps were obtained by projecting the MNI-scalp spline-Laplacians onto one subject's anatomical fMRI image via Tikhonov (L2) regularization, maintaining similar distributions of activity of the surface Laplacians on the cortical surface. Blue and orange regions correspond to areas that produce negative and positive potentials observed on the scalp respectively.

spline-Laplacians (Deng et al., 2012) to a folded cortical surface, which resulted with most amplitude existing on the gyral crowns (i.e. the "smooth" cortex). The surface spline-Laplacians were projected onto a cortical shape generated by an anatomical MRI of a single individual. This individual's brain image had cortical folds that better localized particular regions than the MNI brain shape. Each subject's N200 projection was performed using Tikhonov (L2) regularization to inverse the Finite Element (FE; Pommier and Renard, 2005) forward model based on the MNI 151 average head, maintaining similar spatial-distributions of activity of the surface Laplacians to the cortical surface. Cortical topographic maps of the average N200 waveform across EEG sessions and noise conditions are show in the Bottom panel of **Figure 4**. Each brain vertex was labeled using the Destrieux cortical atlas (Fischl et al., 2004). Locations listed were ones that were found in at least 70% of localizations across EEG sessions and experimental conditions using an empirically found cutoff (estimated at -10 units microamperes per mm^2). However we should note that the localization procedure must have some errors due to between-subject variance in both cortical and cranial shape and between-subject variance in tissue properties. These sources of variance could not easily be accounted for, and remains a source of error in this (and all) cortical projection techniques.

Presence of fast errors in response time distributions

One possible confound in evaluating the relationship between N200 waveforms and response time distributions is the presence of fast errors. That is, fast response time observations that are not due to a decision making process and occur due to another random process (e.g. a "contaminant" process unrelated to the theorized cognitive process). Because these response times are not due to a decision process, the associated accuracy on those trials should be about 50% in a two-alternative forced choice task. Recent research has been performed and researchers have developed theory on the notion of "mind-wandering", which is defined as cognition that departs from that which is useful to the task at hand (e.g. Hawkins et al., 2015; van Vugt et al., 2015; Fox et al., 2015; Lin et al., 2016). Fast errors could be considered a special case of mind-wandering as a subset of contaminant trials. An analysis of other types of contaminant trials and the influence of these trials on the presented analyses is discussed below.

In order to remove fast responses times that were not due to a decision process, an exponentially weighted moving

average was used to calculate accuracy sorted by response time, from shortest response time to longest response time. A cutoff of 60% accuracy was explored such that the accuracy data and the associated short response times were removed from the analysis. However a fixed cutoff of 350 ms yielded no difference in the ultimate results, and therefore a fixed cutoff was maintained in the data. This procedure resulted in less than 7.6% of the trial data being dropped for each visual noise condition in each session of EEG ($N = 147$), with most observations having 0% removed.

Cognitive theory of human decision-making

We tested the relationship between N200 peak-latency and VET directly by fitting response time and choice data from the human subjects to simple drift-diffusion models. In these models, human *visual encoding time* (VET) is the first cognitive processing time after a visual stimulus is displayed and the subject must then make a decision based on the visual input (see **Figure 9**). The *non-decision time* (NDT) τ parameter is the sum of VET and other time-invariant processes across trials not associated with a sequential accumulation of evidence, such as motor execution time (Ratcliff, 1978; Ratcliff and McKoon, 2008). We therefore tested whether the linear relationship between N200 peak-latency and NDT had a slope of 1, reflecting the hypothesis that N200 peak-latency is one additive component of NDT.

We assessed our ability to recover true non-decision time (NDT) estimates from RT percentiles and hierarchical Bayesian model fitting by simulating response time data. Response time data was simulated from drift-diffusion models with various amounts of trial-to-trial variability in NDT, evidence boundary (amount of evidence require to make a decision), and evidence accumulation rate (i.e. drift rate) suggested by Ratcliff (1978). These response times were simulated using DMAT, MATLAB software for simulating and estimating diffusion model parameters (Vandekerckhove and Tuerlinckx, 2008). These simulations revealed that even with the presence of trial-to-trial variability in all cognitive parameters (NDT, evidence boundary, and evidence accumulation rate), means of non-decision time and evidence accumulation rate could still be recovered. In particular, mean NDT across trials was well estimated by 1) 10th percentiles of response time distributions (with about 60 ms of fixed bias in 10th percentiles compared to

true mean NDTs) and 2) hierarchical Bayesian fitting of a simple drift-diffusion model (DDM) with between-session variability in the three free parameters (Wabersich and Vandekerckhove, 2014). Although mean NDTs are not as well estimated in the presence of a large amount of contaminant trials (see Results section and **Figure 8**). These simulations results informed us that both 1) simple regression on the fastest 10% of response times and 2) embedded regression analyses in hierarchical Bayesian models would reflect true relationships between N200 waveforms and cognitive parameters, assuming that the theoretical model of decision making approximates the true cognitive process.

N200 waveforms versus response times

Linear regressions of 1) trial-averaged N200 deflection times and peak-latencies versus 10th response time percentiles across noise conditions in EEG sessions and 2) single-trial N200 peak-latencies versus response times were performed. The fastest response times in each EEG session and noise condition are expected to be the linear sum of *visual encoding time* (VET) and other sequential cognitive processes that are mostly invariant across trials. This is because in any response time process that contains a mix of stochastic evidence accumulation and fixed processes with smaller amounts of variability, NDT (time periods not associated with evidence accumulation during decision making trials, see Voss et al., 2004; Ratcliff and McKoon, 2008) will be reflected in the fastest response times. The fastest response times in each EEG session and noise condition were estimated by the 10th percentile. The 10th percentile was chosen because the smaller percentiles were more likely to include contaminants due to mind-wandering as discussed above (although similar results were empirically found in post-hoc analyses of the 1st percentile RTs).

Linear regression statistics reported are 95% confidence intervals related to the p values and t statistics in the Neyman and Pearson (1933) tradition as well as Bayes Factors (BF) which describe the amount of relative evidence (probability in the Bayesian definition) of a model which has a non-zero regression slope over a model which has a regression slope of zero (Jeffreys, 1961; Kass and Raftery, 1995; Rouder and Morey, 2012). Generally Bayes Factors over 3 are considered positive evidence for an effect (i.e. the effect is 3 times more likely under the alternative hypothesis than the null hypothesis) while over 20 is strong evidence (Kass and Raftery, 1995). Adjusted R^2 is also reported that describes the fraction of variance of the dependent variable (10th response time percentiles or single-trial reaction

times) explained by the regressor variable (measures of neural processing speed). R^2_{adj} ranges from 0 to 1. These statistics were generated by JASP, a open-source graphical software package for statistical analysis (JASP Team, 2017).

Also reported are Bayes Factors (BF1) of a 1-to-1 relationship between response time and N200 measures that describe the amount of relative evidence (e.g. "probability" in the Bayesian definition) of the slope parameter being equal to 1 (e.g. 1 ms increase in N200 peak-latency corresponds to a 1 ms increase in visual encoding time) over a model which has a largely unknown regression slope. That is, the comparison density and prior probability of slope parameter was $\beta \sim \mathcal{N}(1, 3^2)$. BF1 were calculated using the simple Savage-Dickey Density Ratio (Dickey and Lientz, 1970; Wagenmakers et al., 2010) which is the ratio of the height of the posterior distribution over the prior distribution at the tested value. These Bayes Factors were calculated by running simple JAGS code, a program that easily samples from marginal posterior distributions of using Markov Chain Monte Carlo (MCMC; Plummer, 2003). These Bayes Factors, BF1, are typically much smaller than the Bayes Factors used to test the existence of an effect because less data is needed to prove the existence of an effect than to prove the effect is equal to a specific value (slope equal to 1, in this case).

Integrated neuro-cognitive model fitting

Testing the data directly, parameter estimates from three hierarchical Bayesian models were found. These linear relationships were estimated in a single-step in a hierarchical Bayesian framework.

Drift-diffusion modeling was applied to response time and accuracy data from Experiments 1 & 2 jointly, containing between session-differences in NDT τ, evidence accumulation rate δ, and speed accuracy trade-off parameter α that were explained differences in N200 waveform peak-latencies z. All built models were assumed to be hierarchical, describing intrinsic session j, condition k, and experiment e variability which 1) ensured model fits with small amounts of data (Lee, 2008; Lee and Newell, 2011; Vandekerckhove et al., 2011) and 2) provided the ability to describe data more accurately for observed and unobserved subjects in future analyses (Wagenmakers, 2009; Nunez et al., 2017). Bayesian hierarchical drift-diffusion models were fit using Wiener likelihood approximations in JAGS, a program that

can easily sample from hierarchical models using Markov Chain Monte Carlo (MCMC) (Plummer, 2003; Wabersich and Vandekerckhove, 2014) using the pyjags Python package (Miąsko, 2017).

Hierarchical models 1 and 2 had the same base structure on drift-diffusion model parameters with linear regression influence of N200 peak-latency z_{jke} on each parameter, expressed as functions $f(z_{jke})$. Hierarchical model 3 had the same base structure with function $f(z_{jke}) = 0$ on the session j level, but with linear regressions on the single-trial n level discussed below. The base structure of all three models was the following:

$$\tau_{jke} \sim \mathcal{N}(\eta_{(\tau)ke} + f_1(z_{jke}),\ \sigma^2_{(\tau)}) \in (0,1) \quad , \quad \eta_{(\tau)ke} \sim \mathcal{N}(0.3, 0.25^2), \quad \sigma_{(\tau)} \sim \Gamma(0.2,1) \tag{1}$$

$$\delta_{jke} \sim \mathcal{N}(\eta_{(\delta)ke} + f_2(z_{jke}),\ \sigma^2_{(\delta)}) \in (-9,9), \quad \eta_{(\delta)ke} \sim \mathcal{N}(1, 2^2) \quad , \quad \sigma_{(\delta)} \sim \Gamma(1,1) \tag{2}$$

$$\alpha_{jke} \sim \mathcal{N}(\eta_{(\alpha)ke} + f_3(z_{jke}),\ \sigma^2_{(\alpha)}) \in (0.1,3), \quad \eta_{(\alpha)ke} \sim \mathcal{N}(1, 0.5^2) \quad , \quad \sigma_{(\alpha)} \sim \Gamma(1,1) \tag{3}$$

$$z_{jke} \sim \mathcal{N}(\zeta_{ke},\ \sigma^2_{(z)}) \quad , \quad \zeta_{ke} \sim \mathcal{N}(0.2, 0.1^2) \quad , \quad \sigma_{(z)} \sim \Gamma(0.2,1) \tag{4}$$

In Model 1, wide (uninformative) priors were given to the hierarchical effects μ_i of N200 peak-latency on drift-diffusion model parameters i, centered at 1 in order to calculate Bayes Factors (BF1) testing a 1-to-1 relationship using the Savage-Dickey density ratio (Verdinelli and Wasserman, 1995). As a sensitivity analysis, wide priors centered at 0 were used in previous fits of the model, which had inconsequential effects on the parameter estimates (i.e. posterior distributions). The final fit of Model 1 thus had the following embedded linear regression and prior structure:

$$f_i(z_{jke}) = \gamma_{ike} z_{jke} \tag{5}$$

$$\gamma_{ike} \sim \mathcal{N}(\mu_i,\ \sigma^2_{(\gamma)}), \quad \mu_i \sim \mathcal{N}(1, 3^2), \quad \sigma_{(\gamma)} \sim \Gamma(1,1) \tag{6}$$

Model 2 was created in order to test the post-hoc hypothesis that noise condition and visual noise type (differing across the two experiments) modified the effect of N200 peak-latency on NDT. In Model 2, the effect of trial-averaged N200 peak-latency on NDT was assumed to be moderated by noise condition and experiment. The modifying effects tested represented any additional visual noise above low noise θ_{i1}, the effect of high noise θ_{i2}, the effect of Experiment

2 visual noise type θ_{i3}, the interaction effect between any additional noise and Experiment 2 visual noise type θ_{i4}, and the interaction effect between high noise and Experiment 2 visual noise type θ_{i5}. Priors of the modifier effects θ of N200 peak-latency on the drift-diffusion model parameters were centered at 0 in order to calculate Bayes Factors for support of the null hypothesis (BF0) using the Savage-Dickey density ratio (Verdinelli and Wasserman, 1995). Thus Model 2 had the following embedded linear regression and prior structure:

$$f_i(z_{jke}) = \gamma_{ike} z_{jke} + \theta_{i1} z_{jke} + \theta_{i2} z_{jke} + \theta_{i3} z_{jke} + \theta_{i4} z_{jke} + \theta_{i5} z_{jke} \quad (7)$$

$$\gamma_{ike} \sim \mathcal{N}(1, 3^2), \quad \theta_{iike} \sim \mathcal{N}(0, 1^2) \quad (8)$$

In Model 1 Bayes Factors for each effect parameter γ for each visual noise condition and type (i.e. experiment) were calculated using Python and R scripts with the Savage-Dickey density ratio (Verdinelli and Wasserman, 1995) of the posterior density over the prior density at $\gamma = 1$. These Bayes Factors provide the degree of evidence (defined as a probability ratio in Bayesian statistics) of a model where effect of trial-averaged N200 peak-latency on NDT is 1-to-1 versus a model where the effect is unknown (the prior model where $\gamma \sim \mathcal{N}(1, 3^2)$). In **Model 2** Bayes Factors for *additional* effect parameters θ of each visual noise condition and type were calculated with a Savage-Dickey density ratio of the posterior density over the prior density at $\theta = 0$. These Bayes Factors provide the degree of evidence of a null model of no additional N200 effects with increasing visual noise contrast versus a model where the moderator effects are unknown (the prior model where $\theta \sim \mathcal{N}(0, 1^2)$).

Model 3 was fit to find posterior distributions of decision-model parameters for *single-trial* N200 peak-latency linear effects on single-trial NDT (the sum of VET and motor response time as estimated by a hierarchical Bayesian account of a drift-diffusion model). Because of the expected presence of mind-wandering, the results of model fitting simulation, and known caveats with this modeling method (e.g. see Hawkins et al., 2017), it was expected that while the model may uncover a true positive relationship, we would not be able to recover the true effect size with

linear parameters. The model was fit with linear relationships between N200 peak-latencies x on single-trials n and single-trial drift-diffusion model parameters. An exponential around the boundary separation linear equation was used in order to aid in model fitting, reflecting a multiplicative effect on boundary separation instead of a linear effect. Also included were hierarchical linear effect parameters in order to summarize the linear effects for each noise condition and noise type (i.e. experiment). In addition to the base structure presented at the beginning of this section, Model 3 had the following structure (where variable $\mathbf{y}$ refers to the choice and response time on trial n from a drift-diffusion model; DDM):

$$f_i(z_{jke}) = 0 \tag{9}$$

$$\mathbf{y}_{njke} \sim \text{DDM}(\ \tau_{jke} + \lambda_{1jke} x_{njke},\ \delta_{jke} + \lambda_{2jke} x_{njke},\ \exp(\alpha_{jke} + \lambda_{3jke} x_{njke})\ ) \tag{10}$$

$$x_{njke} \sim \mathcal{N}(z_{jke},\ \sigma^2_{(x)}), \quad \sigma_{(x)} \sim \Gamma(0.2, 1) \tag{11}$$

$$\lambda_{ijke} \sim \mathcal{N}(\gamma_{ike},\ \sigma^2_{(\lambda)}), \quad \sigma_{(\lambda)} \sim \Gamma(1, 1) \tag{12}$$

$$\gamma_{ike} \sim \mathcal{N}(\mu_i, \sigma^2_{(\gamma)}), \quad \mu_i \sim \mathcal{N}(1, 3^2), \quad \sigma_{(\gamma)} \sim \Gamma(1, 1) \tag{13}$$

Code Accessibility

Pre-calculated EEG measures, raw behavioral data, MATLAB stimulus code, and MATLAB, Python, R, and JAGS analysis code are available on `https://osf.io/jg9u3/` and in the following repository `https://github.com/mdnunez/encodingN200` (as of March 2018).

Results

Source localization of N200 waveforms

Two interesting findings are suggested by the localization process (see also the Bottom panel of **Figure 4**). One is that the N200 waveforms are distributed across the cortex and not localized to one particular area. This may be reflective of a network that gives rise to the N200 peaks instead of local processing. The second interesting finding is that the N200 peaks are localized more to one side in almost every subject, but not the same side across subjects. While the estimated cortical sources were distributed, the source estimation method described above suggested that N200 peaks in this study could be found primarily in the following cortical locations (such that the locations listed here were present in at least 70% of the localizations across EEG sessions and noise conditions): the middle temporal gyri (both hemispheres), the postcentral gyri (both hemispheres), and the right angular gyrus. The right middle temporal gyrus was the location of the minimum amplitude (i.e. the greatest magnitude of the N200 peak) in 55.8% of observations across EEG sessions and noise conditions. While all other locations contained the minimum amplitude in less than 10% of observations.

Work by Mishkin et al. (1983) and Lamme and Roelfsema (2000), among others, suggest that the segregation of the target Gabor from visual noise would occur in the temporal "segregation" pathway of the primate cortex at about 150 ms (after a delay due to feedforward and feedback visual network behavior). The localization of the N200 waveforms in human extrastriate and temporal locations (especially the right middle temporal gyrus) points to the N200 peak-latency being the time point at which the target Gabor is "segregated" from visual noise in the human cortex, in order to accumulate visual evidence for a motor response. Direct evidence that the N200 peak-latency represents VET, the time before evidence accumulation, is discussed below.

Data summary: N200 deflection, peak-latency, response time and accuracy distributions

Data summarizes of N200 deflection times, trial-averaged N200 peak-latencies, 10th response time percentiles (shown to be a stable but biased estimate of NDT), median response times across trials, and mean accuracy across trials are given in **Table 1**, such that the total sample size of each measure was $N = 147$. A significant but weak correlation

was found between the found N200 deflection times and the N200 peak-latencies ($\rho = .274$, $p < .001$). A significant correlation was found between the N200 peak-latencies and 10th response time percentiles (a less specific test of our main hypothesis; $\rho = .387$, $p < .001$). No correlation was found between the N200 deflection times and 10th response time percentiles ($\rho = -0.086$, $p = .30$). From the data summaries in **Table 1** it is clear that N200 peak-latencies, 10th response time percentiles, and median reaction times generally become longer in higher-contrast noise conditions, an expected effect of visual noise condition on VET (due to more difficult figure-ground segregation). This was not true between the Low and Medium noise conditions in Experiment 1, although it should be noted that there was not much behavioral difference between Low and Medium noise contrast in Experiment 1 in response time nor accuracy. Decreasing accuracies with higher noise contrast are an expected effect of visual noise contrast on decision-making. The effects of visual noise condition on VET versus decision-making time (both components of response time) were separated by the integrated neuro-cognitive modeling results presented below.

There were 14 unique subjects across both experiments (with two subjects participating in both experiments). In order to explore true individual differences, observations of the N200 deflection time, N200 peak-latency, median response time and accuracies were averaged across the two experiments and all conditions for each subject. The range of these measures are given in **Table 2**. All of these measures varied widely across subjects, suggesting individual differences in VET and decision-making time (e.g. response time related to a accumulation of evidence). Some of these individual differences account for the variation observed in N200 deflection times and N200 peak-latencies distributions presented in **Figure 3**. It should be noted that four of the subjects were considered trained on the task, with two subjects completing 9 sessions (both experiments) and two other subjects completing 7 sessions of the second experiment. While not the focus of this particular study, future work should seek to discover if individual differences in VET are explained by individual differences in N200 peak-latencies (a hypothesis expected from the results of the research presented here).

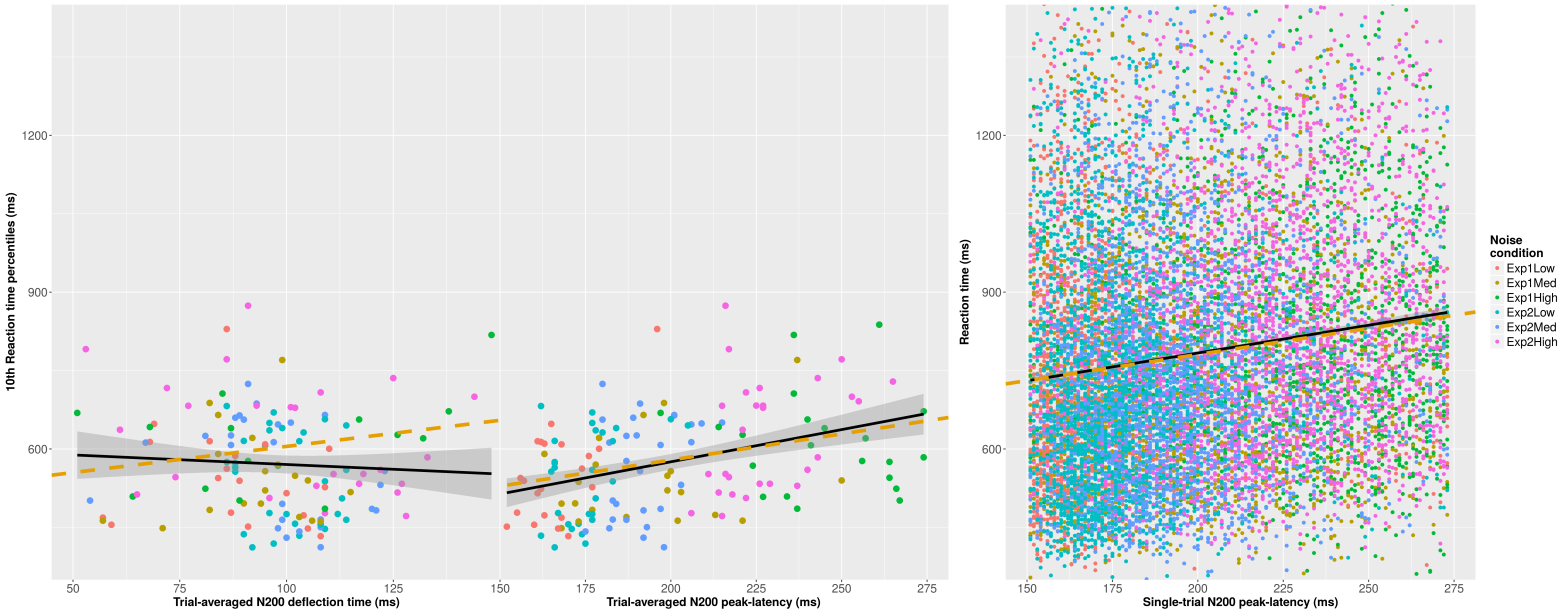

Figure 5. Left: A scatter plot of trial-averaged N200 deflection times and 10th response time percentiles (an estimate of the processing time of time-invariant cognition across trials; NDT) Middle: A scatter plot of trial-averaged N200 peak-latencies and 10th response time percentiles. Observations were generated per noise condition and per EEG collection session ($N = 147$). Right: A scatter plot of single-trial N200 latencies versus single-trial response times. Observations were generated per trial ($N = 13{,}426$). Best-fit simple linear regression lines are shown in black with 95% confidence intervals for the intercept and slope parameters shown in gray. Overlaid on the linear regression lines are gold dashed lines representing the hypothesis with a slope of 1. That is, the expected influence of N200 peak-latency on response time is 1-to-1 millisecond if N200 peak-latency reflected human visual encoding time (VET).

Data summary across unique EEG sessions ($N = 49$) and conditions (total $N = 147$)

		N200 Deflection times	N200 Peak-latencies	10^{th} Percentile Response times	Median Response times	Mean Accuracy
	Overall Mean	95.5 ms	199.6 ms	575.0 ms	852.8 ms	78.76%
	5^{th} Percentile	48.3 ms	162.0 ms	443.6 ms	629.5 ms	58.36%
	Median	97.0 ms	192.0 ms	562.4 ms	845.8 ms	78.76%
	95^{th} Percentile	136.5 ms	259.8 ms	733.6 ms	1139.5 ms	95.32%
Experiment 1	Low Noise Mean	81.9 ms	166.3 ms	549.1 ms	833.0 ms	72.25%
	Medium Noise Mean	94.0 ms	193.0 ms	541.9 ms	821.3 ms	70.14%
	High Noise Mean	108.2 ms	244.5 ms	613.0 ms	896.8 ms	61.77%
Experiment 2	Low Noise Mean	100.1 ms	175.0 ms	545.3 ms	809.1 ms	90.07%
	Medium Noise Mean	93.6 ms	192.2 ms	565.3 ms	829.7 ms	89.59%
	High Noise Mean	94.5 ms	228.0 ms	629.9 ms	925.3 ms	80.72%

Table 1. Summary statistics for each data type used in this study across both EEG sessions and visual noise conditions for a total sample size of 147. Experiment 1 had a sample size of 63 (21 unique EEG sessions per visual noise condition). Experiment 2 had a sample size of 84 (28 unique EEG sessions per visual noise condition). N200 peak-latencies, 10th percentile response times, and median response times become longer in more difficult (lower accuracy) noise conditions. This is not true of N200 deflection times in Experiment 2. VET is expected to become longer when segregation of the visual target is more difficult in conditions of high noise contrast.

Simple results: Scatter plots and linear regression

In order to explore the hypothesis that trial-averaged N200 peak-latency predicts session-level visual encoding time (VET), linear models between N200 peak-latencies and 10th response time percentiles (both correct and incorrect response times combined) were fit. In evidence accumulation models of quick decision making, the *shifts* of response

Data summary across unique subjects ($N = 14$)

	N200 Deflection times	N200 Peak-latencies	10^{th} Percentile Response times	Median Response times	Mean Accuracy
Minimum	57.7 ms	183.2 ms	482.3 ms	649.1 ms	62.67%
Mean	91.7 ms	199.5 ms	567.3 ms	839.7 ms	72.33%
Maximum	129.2 ms	225.3 ms	676.2 ms	1070.8 ms	90.14%

Table 2. Summary statistics for each data type averaged within each of the 14 unique subjects. All measures varied widely across subjects suggesting individual differences in VET and other decision-related cognitive processes.

time (RT) distributions (and thus the small RT percentiles) should correlate with NDT (i.e. VET + residual motor response time) while the shape of RT distributions (and thus the medium and larger RT percentiles) should correlate both with NDT *and* decision-making processes. Thus linear regressions can be explored without fitting decision-making models to data directly. Using simple linear regression, a close to 1-to-1 relationship was found between trial-averaged N200 latencies and 10th RT percentiles as shown in the middle portion of **Figure 5** with a regression coefficient of $\beta_1 = 1.23$ ($N = 147$, 95% confidence interval: $[0.75, 1.72]$, $p < .001$, $t = 5.05$, BF $= 10.84 * 10^3$, BF1 $= 7.40$). Although it should be noted that only 14% of the variance in 10th RT percentiles were explained by the variance across trial-averaged N200 latencies ($R^2_{adj} = .144$). This latter finding might be expected if other trial-invariant mechanisms besides visual encoding time (VET) contribute to the variance in NDT, such as residual motor response.

The relationship is also expected to be observed on single-trials, albeit with more variance around the regression line. Single-trial estimates of N200 latencies were compared to response times across all data points. Again, a close to 1-to-1 relationship was found between single-trial N200 peak-latencies and response times as shown in the right portion of **Figure 5** with a regression coefficient of $\beta_1 = 1.06$ ($N = 13{,}426$, 95% confidence interval: $[0.94, 1.19]$, $p < .001$, $t = 16.88$, BF $= 2.93 * 10^{59}$, BF1 $= 25.91$). However only about 2% of the variance of raw single-trial response times were explained ($R^2_{adj} = .021$). This is expected since other mechanisms besides visual encoding time

(VET) should contribute to the variance in response times on single trials, which was explored with the following cognitive modeling results.

No relationship was found between N200 deflection times across trials and 10th RT percentiles ($N = 147$, $p = .301$, $t = -1.04$, BF $= 0.29$, BF1 $< .001$). The linear regression is shown in the left portion of **Figure 5**. In fact, the Bayes Factor BF1 displayed evidence strongly in favor of $\beta_1 \neq 1$ ($1/\text{BF1} = 225.96$). This suggests that while N200 deflection times may reflect an early visual processing stage, variance in N200 deflection times across noise conditions and EEG sessions does not correspond with variance in response time distribution shifts across noise conditions and EEG sessions.

Modeling results: Embedded linear relationships with decision-making parameters

Each model was fit using JAGS with six Markov Chain Monte Carlo (MCMC) chains of 52,000 samples each run in parallel with 2,000 burn-in samples and a thinning parameter of 10 resulting in 5,000 posterior samples in each chain. The posterior samples from each chain were combined to form one posterior sample of 30,000 samples for each parameter. Model convergence was evaluated based on the Gelman-Rubin statistic $\hat{R}$, which compares the estimated between-chains and within-chain variances for each model parameter (Gelman and Rubin, 1992). Using this statistic all three models were judged to have converged, with $\hat{R} \leq 1.03$ for all parameters in each model ($\hat{R} > 1.10$ for any parameter is usually deemed evidence for a lack of convergence of the entire model fit).

Model 1 was used to evaluate the effect of trial-averaged N200 peak-latency on NDT across EEG sessions and noise conditions. The mean effect across all conditions of each experiment μ_γ provides a sense of how N200 peak-latency tracks NDT τ in general. The posterior distribution of this parameter was found to be around 1 in each condition and experiment as shown in **Figure 6**, indicating that 1 ms increase in N200 processing corresponded to a roughly 1 ms increase in NDT. The posterior distribution of the overall hierarchical effect of N200 peak-latency on NDT across sessions is plotted at the top of **Figure 6**, indicating that the overall Bayes Factor for a 1-to-1 relationship between N1 latency and NDT is BF1 $= 4.90$, reflecting moderate evidence (median = 0.67, 95% credible interval: $[-0.13, 1.66]$). However all the posterior distributions are centered below 1 for each unique noise condition. The reason that the

center of the posterior distributions were below 1 was thought to be due to contaminant trials and is discussed in the next section. The effects of N200 peak-latency on two decision-making parameters was also explored in order to disentangle the three cognitive parameters. An undetermined effect of trial-averaged N200 peak-latency on evidence accumulation rate δ was found (median = -3.23 evidence units per second, 95% credible interval: $[-6.53, 0.16]$). However there may be a positive effect of trial-averaged N200 peak-latency on boundary separation α (median = 1.59 evidence units per second, 95% credible interval: $[0.09, 3.06]$), assuming that boundary separation is well estimated.

Model 2 was fit post-hoc in order to evaluate the observed modifying effect of noise condition on the linear effect of N200 peak-latency on cognitive parameters (see increasing trend across conditions in **Figure 6**). The results were inconclusive. Not much evidence was found for the null models as indicated by the Bayes Factors near 1 for the null effects $BF0$ as shown in **Figure 7**. However, not much evidence exists for *the existence* of moderator effects θ either (existence for moderator effects in this formulation would be $BF0$ much smaller than 1). The base effect posterior distribution (evidence for the effect of N200 peak-latency on NDT in Experiment 1 in the low noise condition) was close to that of the overall effect posterior in Model 1 (BF1 = 4.46, median = 1.18, 95% credible interval: $[-0.12, 2.54]$). Undetermined effects of trial-averaged N200 peak-latency on evidence accumulation rate (median = -2.85 evidence units per second, 95% credible interval: $[-6.34, 0.71]$) and boundary separation (median = 1.28 evidence units per second, 95% credible interval: $[-0.74, 3.46]$) were found that were not differentiable from no effects.

Model 3 was fit in order to evaluate the effect of single-trial N200 peak-latency on non-decision time for each EEG session. In Model 3, the hierarchical effect parameter μ_γ provides a sense of how *single-trial* N200 peak-latency effects NDT. This parameter suggested that the overall single-trial effect was positive (median = 0.23, 95% credible interval: $[0.02, 0.44]$), but no evidence was found that this single-trial effect was equal to 1 (BF1 $< .001$; reflecting that there was *not* a 1-to-1 correspondence on single-trials between N200 peak-latency and NDT). This result may be expected with the presence of unremoved contaminant trials in drift-diffusion model fits (see section below). Undetermined effects of single-trial N200 peak-latency on evidence accumulation rate (median = -0.40 evidence units per second, 95% credible interval: $[-1.72, 0.97]$) and boundary separation (median = 0.25 evidence units per second, 95% credible

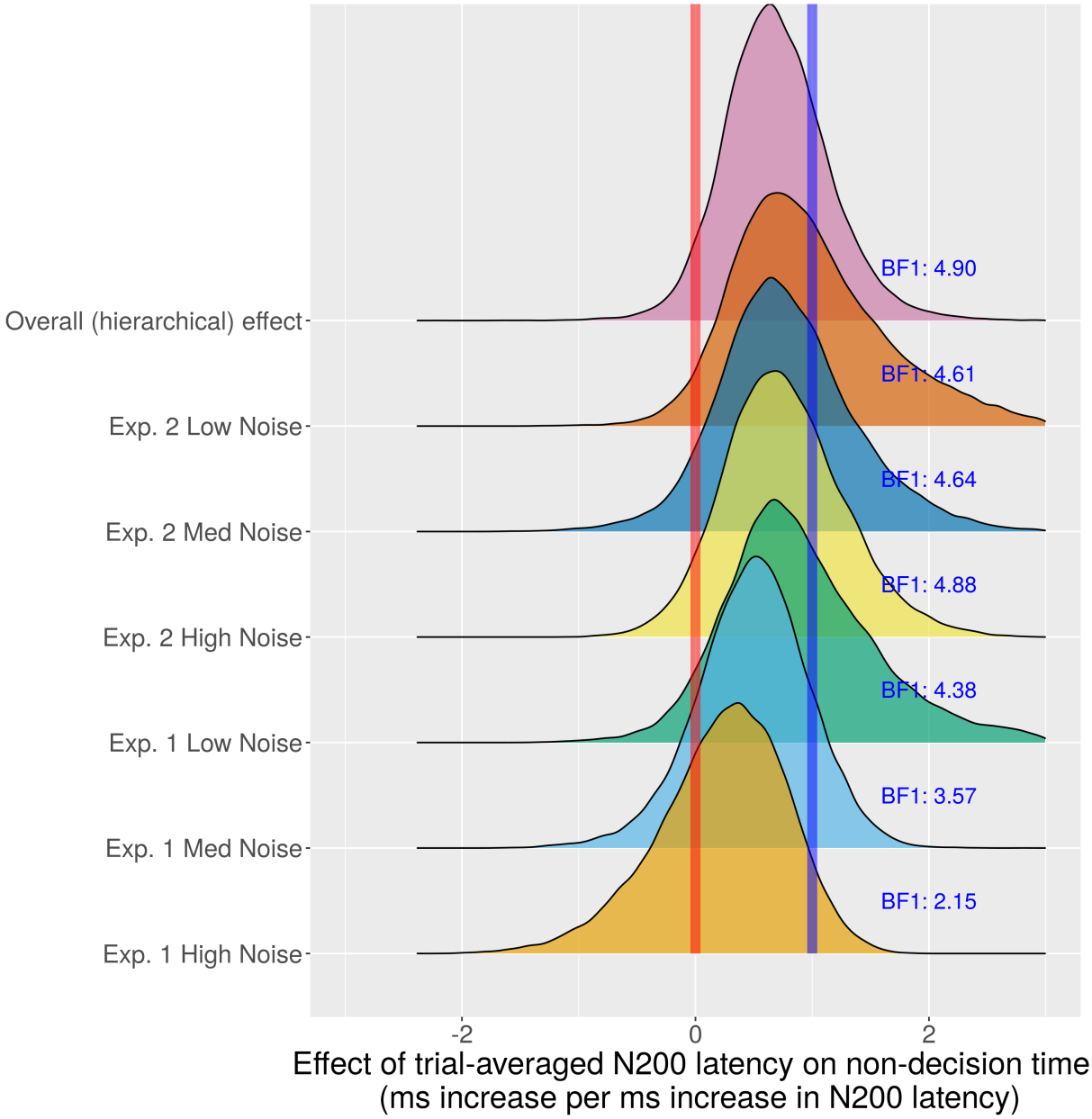

Figure 6. Posterior distributions (Model 1) of effects of N200 peak-latency on non-decision time (NDT). Posterior distributions provide measures of parameter uncertainty in Bayesian model-fitting methods. If the posterior distributions had most of their density around the blue line, this would be strong evidence for the 1-to-1 relationship when the model assumptions are true. Posterior distributions with most of their density around the blue line would be evidence for the true effect equaling 1. Posterior distributions with most of their density around the red line would be strong evidence for the null hypothesis (the parameter equals 0). Some evidence exists for the effects of N200 peak-latency on NDT to be 1-to-1 (one millisecond increase in N200 peak-latency corresponds to a millisecond increase in NDT) as indicated by the Bayes Factors calculated with a Savage-Dickey density ratio (Verdinelli and Wasserman, 1995) of the posterior density over the prior distribution at $\gamma = 1$.

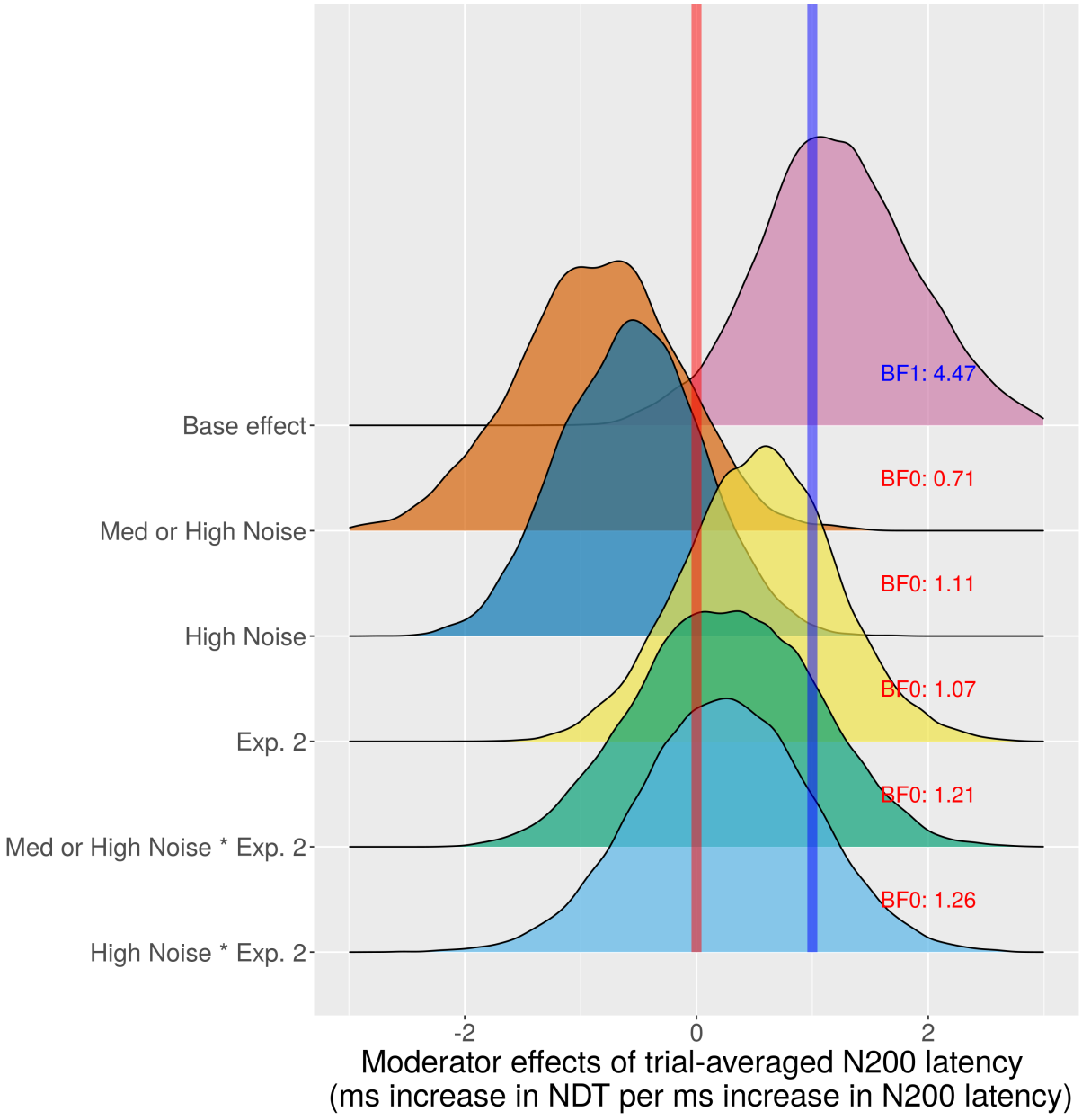

Figure 7. Posterior distributions (Model 2) of the *additional* effects (i.e. *moderator* effects) for each unique visual noise condition of N200 peak-latency on non-decision time (NDT). Posterior distributions provide measures of parameter uncertainty in Bayesian model-fitting methods. Posterior distributions with most of their density around the blue line would be evidence for the true effect equaling 1. Posterior distributions with most of their density around the red line would be strong evidence for the null hypothesis (the parameter equals 0). Evidence for the base effect of N200 peak-latency on NDT being 1-to-1 is similar to the results of Model 1 (top posterior distribution). The tests for moderator effects were inconclusive (all other posterior distributions). Not much evidence exists for moderator effects of condition. There is also not much evidence for *no* moderator effects as indicated by the Bayes Factors for the null effects *BF* near 1.

interval: $[-0.24, 0.78]$) were found that were not differentiable from no effect.

Simulations with contaminant trials

The simulations presented in the Methods section revealed that the model can still recover some true NDTs on the EEG session level with the presence of "contaminant" trials. That is, some trials were expected to be from processes other than decision-making (i.e. "contaminant processes" for cognitive model fitting). These "mind-wandering" processes were simulated such that the amount of trials with processes unrelated to decision-making (e.g. see Hawkins et al., 2015) was systematically varied. The ability to recover accurate estimates of NDTs from 10th percentiles and the hierarchical Bayesian fitting procedure with JAGS (Plummer, 2003; Wabersich and Vandekerckhove, 2014) was assessed by quantifying the regression slope between true NDT and estimated NDT. It was hypothesized that the regression slope between true NDT and estimated NDT would be less in trials with more contaminant processes that were not removed from the 350 millisecond cutoff (e.g. to remove fast errors). This was a post-hoc hypothesis that evaluated the reasons for a slope less than 1 in high noise contrast trials between trial-averaged N200 peak-latency and estimated NDT (see **Figure 6**).

The simulations suggested the presence of more contaminant trials resulted in slope parameters less than 1, but that 10th percentiles better reflect true NDT across subjects (although they overestimate NDTs by approximately 60 ms) and therefore would be more immune to contaminant processes than estimates from simple drift-diffusion modeling. Therefore if N200 peak-latency reflected a true additive NDT process (i.e. visual encoding time; VET) this would explain the strong evidence of a 1-to-1 relationship in the linear regressions of N200 peak-latency and 10th RT percentiles (**Figure 5**) but weaker (although still present) evidence of a 1-to-1 relationship between N200 peak-latency and estimated NDTs when fitting drift-diffusion models directly (**Figure 6**). It should be noted that VET is only one theorized process of estimated NDT, but that the addition of uncorrelated non-decision cognitive processes to NDT would not affect linear regressions between VET and true NDT besides additional uncorrelated noise.

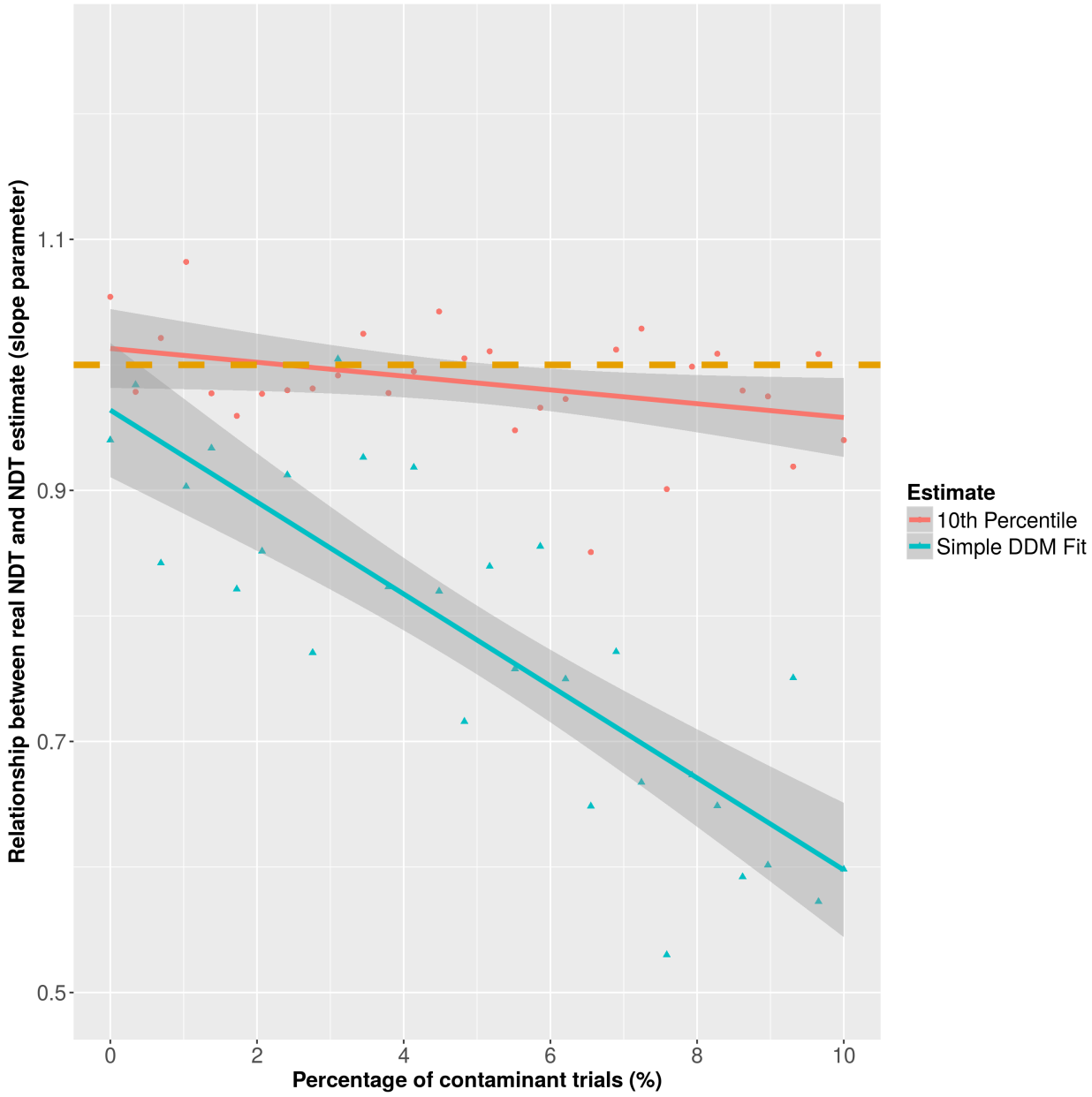

Figure 8. The addition of more trials from contaminant processes resulted in some non-decision time (NDT) estimates being negatively biased towards smaller values. This, in turn, resulted in decreased linear relationships (e.g. less than 1-to-1) between true NDT and estimated NDT. This was especially true for the estimates of simple drift-diffusion (DDM) model parameters. This simulation suggested that while 10th response time percentiles were positively biased as estimates of true NDT (e.g. true NDT were approximately 60 ms shorter than the 10th response time percentiles), the 1-to-1 relationship could be well estimated by the 10th percentiles but not the DDM fitting procedure when there were greater than 1% of trials with an unremoved contaminant process. This fact explains why a true measure of VET, such as the proposed N200 peak-latency, might not track DDM-estimated NDT as well as the 10th response time percentiles.

Discussion

Evidence FOR N200 peak-latencies tracking visual encoding time

Both simple regression analyses yielded evidence for a relationship between EEG measures of neural processing speed (N200 waveforms) and visual encoding times (VET). These regression fits indicate that there was 1) approximately a 1 ms increase in response times when there was a 1 ms increase in single-trial N200 peak-latency and 2) approximately a 1 ms increase in the 10th percentile of response times, an estimate of cognitive non-decision time (NDT), when there was a 1 ms increase in trial-averaged N200 peak-latencies across all visual noise conditions and all experimental sessions of EEG. Furthermore, moderate evidence was found of this 1-to-1 relationship of trial-averaged N200 peak-latency on NDT in hierarchical drift-diffusion Models 1 and 2.

These findings match previous research. Our findings in this study closely match findings discussed by Thorpe et al. (1996); Martin et al. (2010); Zhang et al. (2016); Loughnane et al. (2016) as discussed in the Introduction of this paper. In addition, Stanford et al. (2010) showed that when evidence accumulation was blocked for only 100 ms after target onset, monkeys were able to complete their decision, while when evidence accumulation was blocked for 200 ms after target onset, the monkeys were at chance accuracy. This work suggested that visual encoding time must take somewhere between 100 ms and 200 ms for a simple color discrimination task. N200 peak-latencies reflecting visual encoding time would also explain why N200 latencies have been found to engage bottom-up, top-down attention, and a visual attention discriminating process (Vogel and Luck, 2000). In this study we found significant noise-condition effects in N200 peak-latency (see **Table 1**) such that N200 peak-latencies become longer with larger amounts of visual noise contrast (this finding was not observed in the N200 deflection times), and it is expected the VET should become longer with larger amounts of visual noise due to a higher cognitive difficulty of target-noise (e.g. figure-ground) segregation. Furthermore we found significant individual differences in N200 peak-latencies across subjects, which matches expectations that individual differences in cognitive processing exists that explains individual differences in behavior (e.g. see Schubert et al., 2017).

Evidence AGAINST N200 peak-latencies tracking visual encoding time

When exploring the relationship between N200 peak-latencies and non-decision times (NDT) directly with drift-diffusion modeling (DDM), the ability of ERP latencies to reflect visual encoding times (VET) seems to depend upon the quality of visual stimuli. In two experiments with different noise types, the effects of N200 peak-latency differences on NDT differences (assumed to be the sum of VET and residual motor response time) across EEG sessions seemed to be mediated by the contrast condition of the visual distractors. This suggests that how well the peak neural signal latency tracks VET is dependent upon the quality of the external signal itself. Although, not much evidence was found for this qualitative finding as indicated by the Bayes Factors of the null models in **Figure 7**.

The seemingly different N200 peak-latency to NDT relationships across experimental conditions could instead suggest there is a larger presence of "contaminant" response times in high noise conditions that effect estimates of NDT (such as trials when the subject is not focused on the task–dubbed "mind-wandering" by the Cognitive Neuroscience field, e.g. Hawkins et al., 2015; Fox et al., 2015). Simulations revealed that NDTs were not as well estimated when more contaminant trials were introduced. And that the 1-to-1 relationship between true VETs and estimated NDTs were not as robust. This was due to the presence of negatively biased estimates of NDT when more contaminant trials occurred. That is, true NDT was larger than was estimated for some subjects, this in turn decreased the slope of the relationship between true NDT and NDT estimates (see **Figure 8**). Evidence has previously been found that larger amounts of mind-wandering (and thus contaminant trials) can occur in more difficult task conditions (Feng et al., 2013), which would explain why the relationship was closer to 1-to-1 in easier noise conditions. However, while the 10th response time percentile estimates of NDT were biased, they were not as influenced by the addition of contaminant processes. This explains why the relationship between N200 latencies and 10th percentile estimates remained 1-to-1 across all experimental conditions.

Single-trial N200 latencies may not be related to VET in high noise conditions. However, further work is required to find better, testable estimates of single-trial neural processing speed as measured by ongoing EEG. It is also possible that the single-trial N200 latencies *do* give a satisfactory account of VET but fitting simple drift-diffusion parameter relationships fails on single-trials (see Hawkins et al., 2017), especially with the presence of contaminant processes.

This would explain why we found a near 1-to-1 relationship between single-trial N200 peak-latencies and response times (see **Figure 5**) but no evidence of this 1-to-1 relationship (albeit significant and positive relationship) when fitting DDM parameters to N200 peak latencies on single trials. Better theoretical models of behavior with trial-to-trial variability in NDT are probably needed (see Boehm et al., 2018), such as cognitive models that include both decision processes and mind-wandering processes (e.g. see van Vugt et al., 2015; Mittner et al., 2016).

A neuro-cognitive theory of decision making

A neuro-cognitive model of encoding, evidence accumulation, and motor response is proposed that is identified with separable measures of VET and motor response that are estimated from observed EEG, accuracy, and response time distributions. Fitting this type of model to data would allow direct hypothesis testing of observed trial-to-trial differences and individual differences in neural signals as well as human behavior during quick decision making.

Neuro-cognitive hierarchical models of VET, evidence accumulation, and motor response time become identifiable when treating EEG measures (e.g. N200 peak-latencies) as measures of VET. The theory is an extension of a specific class of decision-making models (e.g. "drift-diffusion" models, see Ratcliff and McKoon, 2008, for a review) which predicts that response time and accuracy are explained by a continuous accumulation of evidence towards certain pre-decided evidence thresholds (see **Figure 9**).

A drift-diffusion model of accuracy ($w = 0$ or $w = 1$) and response time t on one trial is predicted to be a function of VET τ_e, motor response time τ_m, the drift rate which is the average rate of evidence accumulation within one trial δ, the diffusion coefficient ς which is the variance around the average rate of evidence accumulation within a trial, and the amount of evidence required to make a decision α_t, which may be assumed to decrease with time. The bias towards correct or incorrect responses is assumed to be equal to $z_0 = 0.5\alpha_t$. The joint density f of RT t and accuracy w of this simplified diffusion model is given in **Equation 14**. The density is derived from the solution given by Ratcliff (1978); Tuerlinckx (2004).

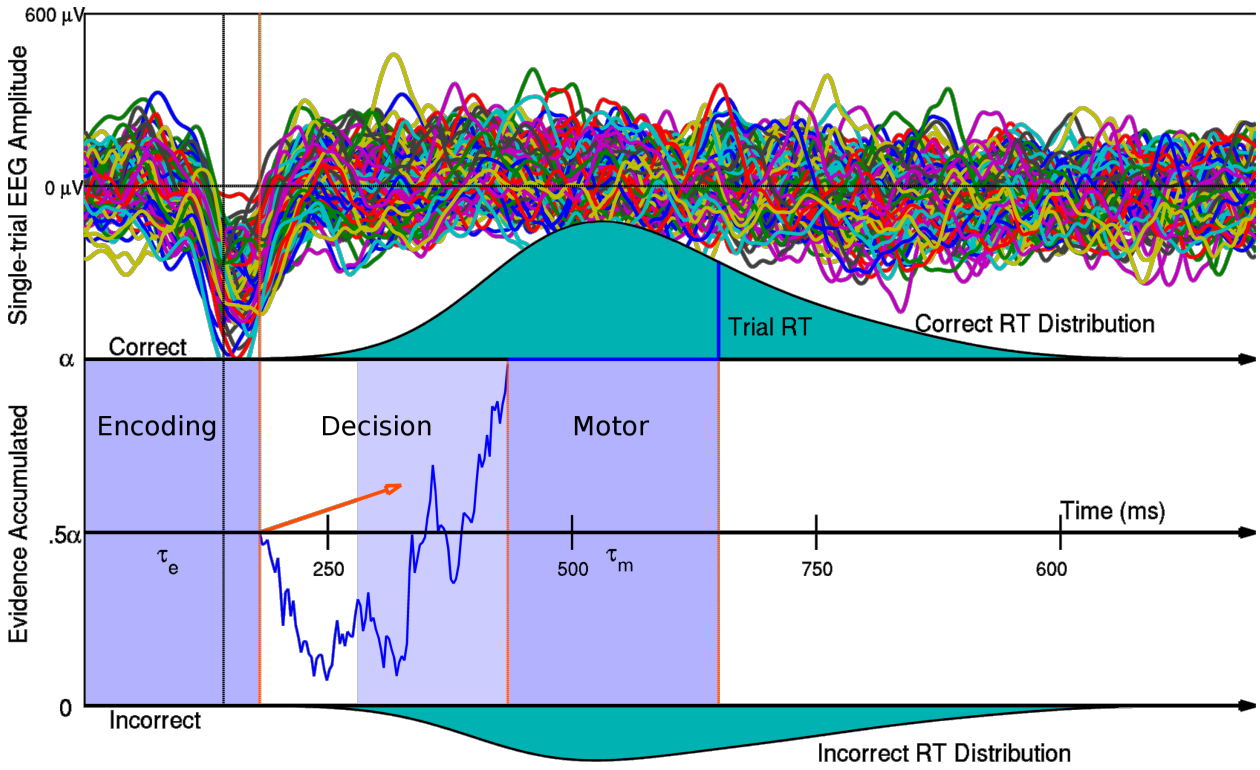

Figure 9. A graphical illustration of a Neural Drift Diffusion model in which the visual encoding time τ_e on single-trials describes the latency of the negative peaks of the N200 waveform on 146 experimental trials. Single-trial observations of the N200 peak-latency are found by using a decomposition of the average ERP response at each electrode and then biasing the raw EEG by the resulting channel weights. Total NDT τ reflects both visual encoding time (VET) τ_e as well as residual motor response τ_m (e.g. motor execution time after the decision is made) and can be estimated from response time distributions. Decision time is generated via a Brownian motion evidence accumulation process with evidence accumulation rate δ (drift rate), evidence accumulation noise ς (diffusion coefficient), and evidence threshold (boundary parameter) α (for more information see Ratcliff, 1978; Ratcliff and McKoon, 2008; Nunez et al., 2015, 2017)

$$\begin{cases} f(t, w=0 \mid \alpha, \varsigma^2, \tau_e, \tau_m, \delta) = \frac{\pi\varsigma^2}{\alpha_t^2} e^{-\frac{1}{2\varsigma^2}\left[\delta\alpha_t + \delta^2(t-\tau_e-\tau_m)\right]} \sum_{k=1}^{\infty} \left[k \sin\left(\frac{1}{2}\pi k\right) e^{-\frac{1}{2\alpha_t^2}k^2\pi^2\varsigma^2(t-\tau_e-\tau_m)} \right] \\ \\ f(t, w=1 \mid \alpha, \varsigma^2, \tau_e, \tau_m, \delta) = f(t, w=0 \mid \alpha, \varsigma^2, \tau_e, \tau_m, -\delta) \end{cases} \tag{14}$$

Note that the density in **Equation 14** is classically unidentifiable when estimating the model with only response time and accuracy observations for two reasons. 1) Encoding time τ_e and motor response time τ_m both contribute to residual response time $\tau = \tau_e + \tau_m$ which approximately equals the smallest observed response times that are not due to contaminant trials. 2) Only two of the three parameters related to evidence accumulation (i.e. drift rate δ, the diffusion coefficient ς, and the boundary separation α) can be found with behavioral data alone. For example, if α_t is constant with t, multiplying ς by two and dividing both α and δ by two would result in the same fit of choice-RT (Wabersich and Vandekerckhove, 2014).

The additive model of VET, evidence accumulation time, and residual motor response time (e.g. motor execution time) suggests that residual motor response time is estimable from the information given in **Table 1**. That is NDT is estimated by the 10th response time percentiles with approximately 60 milliseconds of bias. This means that subtracting 10th response time percentiles by N200 peak latencies (evidenced to track VET from the results in this paper) and 60 milliseconds produces estimates of residual motor response time. This suggests that residual motor response is around 300 milliseconds in each noise condition that is not clearly dependent upon the visual noise condition (322.8 ms, 288.9 ms, 308.5 ms, 310.3 ms, 313.1 ms, and 341.9 ms for Experiments 1 then 2, Low to High noise respectively). Future work will seek to compare these time estimates to EEG motor preparation signals.

Fitting cognitive neuroscientific results to cognitive models is a growing field of research (Mulder et al., 2014; Turner et al., 2015; de Hollander et al., 2016; Turner et al., 2017; Nunez et al., 2017). The goal of future work is to further develop theory that reconciles psychological phenomena with observations about the human brain found in the cognitive neuroscience literature. This work would lead to the ability to fit the density given in **Equation 14** with *identifiable* parameters that explain both psychological phenomena and observed brain electrophysiology. This would

allow researchers to fit the full model to experimental data and give researchers the ability to directly test hypotheses about the cognitive and computational underpinnings behind observed human brain behavior in both healthy and clinical populations.

References

Bach M, Meigen T (1992) Electrophysiological correlates of texture segregation in the human visual evoked potential. *Vision research* 32:417–424.

Boehm U, Annis J, Frank M, Hawkins G, Heathcote A P, Kellen D, Krypotos AM, Lerche V, Logan GD, Palmeri T, Ravenzwaaij Dv, Servant M, Singmann H, Starns J, Voss A, Wiecki T, Matzke D, Wagenmakers EJ (2018) Estimating between-trial variability parameters of the diffusion decision model .

de Hollander G, Forstmann BU, Brown SD (2016) Different ways of linking behavioral and neural data via computational cognitive models. *Biological Psychiatry: Cognitive Neuroscience and Neuroimaging* 1:101–109.

Deng S, Winter W, Thorpe S, Srinivasan R (2012) Improved surface laplacian estimates of cortical potential using realistic models of head geometry. *IEEE Transactions on Biomedical Engineering* 59:2979–2985.

Dickey JM, Lientz BP (1970) The weighted likelihood ratio, sharp hypotheses about chances, the order of a markov chain. *The Annals of Mathematical Statistics* 41:214–226.

Dmochowski JP, Norcia AM (2015) Cortical components of reaction-time during perceptual decisions in humans. *PloS one* 10:e0143339.

Feng S, D'Mello S, Graesser AC (2013) Mind wandering while reading easy and difficult texts. *Psychonomic Bulletin & Review* 20:586–592.

Fischl B, van der Kouwe A, Destrieux C, Halgren E, Ségonne F, Salat DH, Busa E, Seidman LJ, Goldstein J, Kennedy D et al. (2004) Automatically parcellating the human cerebral cortex. *Cerebral Cortex* 14:11–22.

Fox KCR, Spreng RN, Ellamil M, Andrews-Hanna JR, Christoff K (2015) The wandering brain: Meta-analysis of functional neuroimaging studies of mind-wandering and related spontaneous thought processes. *Neuroimage* 111:611–621.

Gelman A, Rubin DB (1992) Inference from iterative simulation using multiple sequences. *Statistical Science* pp. 457–472.

Gold JI, Shadlen MN (2007) The neural basis of decision making. *Annual Review of Neuroscience* 30:535–574.

Hawkins GE, Mittner M, Boekel W, Heathcote A, Forstmann BU (2015) Toward a model-based cognitive neuroscience of mind wandering. *Neuroscience* 310:290–305.

Hawkins GE, Mittner M, Forstmann BU, Heathcote A (2017) On the efficiency of neurally-informed cognitive models to identify latent cognitive states. *Journal of Mathematical Psychology* 76:142–155.

JASP Team (2017) JASP (Version 0.8.1.2) [Computer software].

Jeffreys H (1961) *Theory of probability* Oxford University Press.

Kass RE, Raftery AE (1995) Bayes factors. *Journal of the American Statistical Association* 90:773–795.

Kayser J, Tenke CE (2003) Optimizing PCA methodology for ERP component identification and measurement: theoretical rationale and empirical evaluation. *Clinical Neurophysiology* 114:2307–2325.

Kayser J, Tenke CE (2015) Issues and considerations for using the scalp surface Laplacian in EEG/ERP research: A tutorial review. *International Journal of Psychophysiology* 97:189–209.

Lamme VAF (1995) The neurophysiology of figure-ground segregation in primary visual cortex. *Journal of Neuroscience* 15:1605–1615.

Lamme VAF, Roelfsema PR (2000) The distinct modes of vision offered by feedforward and recurrent processing. *Trends in neurosciences* 23:571–579.

Lamme VAF, Zipser K, Spekreijse H (2002) Masking interrupts figure-ground signals in v1. *Journal of cognitive neuroscience* 14:1044–1053.

Lee MD (2008) Three case studies in the Bayesian analysis of cognitive models. *Psychonomic Bulletin & Review* 15:1–15.

Lee MD, Newell BJ (2011) Using hierarchical Bayesian methods to examine the tools of decision-making. *Judgment & Decision Making* 6.

Lin CT, Chuang CH, Kerick S, Mullen T, Jung TP, Ko LW, Chen SA, King JT, McDowell K (2016) Mind-wandering tends to occur under low perceptual demands during driving. *Scientific Reports* 6.

Loughnane GM, Newman DP, Bellgrove MA, Lalor EC, Kelly SP, OConnell RG (2016) Target selection signals influence perceptual decisions by modulating the onset and rate of evidence accumulation. *Current Biology* 26:496–502.

Luck SJ (2012) Event-related potentials In Cooper H, Camic PM, Long DL, Panter AT, Rindskopf D, Sher KJ, editors, *APA Handbook of Research Methods in Psychology: Volume 1, Foundations, Planning, Measures, and Psychometrics*. American Psychological Association.

Makeig S, Bell AJ, Jung TP, Sejnowski TJ (1996) Independent component analysis of electroencephalographic data. *Advances in Neural Information Processing Systems* 8:145–151.

Martin T, Huxlin KR, Kavcic V (2010) Motion-onset visual evoked potentials predict performance during a global direction discrimination task. *Neuropsychologia* 48:3563–3572.

Miąsko T (2017) pyjags (version 1.2.2) [computer software] `https://github.com/tmiasko/pyjags`.

Mishkin M, Ungerleider LG, Macko KA (1983) Object vision and spatial vision: two cortical pathways. *Trends in neurosciences* 6:414–417.

Mittner M, Hawkins GE, Boekel W, Forstmann BU (2016) A neural model of mind wandering. *Trends in cognitive sciences* 20:570–578.

Mulder MJ, van Maanen L, Forstmann BU (2014) Perceptual decision neurosciences a model-based review. *Neuroscience* 277:872–884.

Neyman J, Pearson ES (1933) On the problem of the most efficient tests of statistical hypotheses. *Philosophical Transactions of the Royal Society of London. Series A, Containing Papers of a Mathematical or Physical Character* 231:289–337.

Nunez MD (2017) Refining understanding of human decision making by testing integrated neurocognitive models of EEG, choice and reaction time Ph.D. diss., University of California, Irvine.

Nunez MD, Horton C, Deng S, Winter W, Srinivasan R (2017) artscreenEEG (version 0.3.0) [computer software] `https://github.com/mdnunez/artscreenEEG`.

Nunez MD, Nunez PL, Srinivasan R (2016) Electroencephalography (EEG): neurophysics, experimental methods, and signal processing In Ombao H, Linquist M, Thompson W, Aston J, editors, *Handbook of Neuroimaging Data Analysis*, pp. 175–197. Chapman & Hall/CRC.

Nunez MD, Srinivasan R, Vandekerckhove J (2015) Individual differences in attention influence perceptual decision making. *Frontiers in Psychology* 6:18.

Nunez MD, Vandekerckhove J, Srinivasan R (2017) How attention influences perceptual decision making: Single-trial EEG correlates of drift-diffusion model parameters. *Journal of Mathematical Psychology* 76, Part B:117–130.

Nunez PL, Pilgreen KL (1991) The spline-laplacian in clinical neurophysiology: a method to improve EEG spatial resolution. *Journal of Clinical Neurophysiology* 8:397–413.

Nunez PL, Silberstein RB, Cadusch PJ, Wijesinghe RS, Westdorp AF, Srinivasan R (1994) A theoretical and experimental study of high resolution EEG based on surface laplacians and cortical imaging. *Electroencephalography and Clinical Neurophysiology* 90:40–57.

Nunez PL, Srinivasan R (2006) *Electric Fields of the Brain: The Neurophysics of EEG* Oxford University Press.

O'Connell RG, Dockree PM, Kelly SP (2012) A supramodal accumulation-to-bound signal that determines perceptual decisions in humans. *Nature Neuroscience* 15:1729–1735.

Parra LC, Spence CD, Gerson AD, Sajda P (2005) Recipes for the linear analysis of EEG. *Neuroimage* 28:326–341.

Philiastides MG, Heekeren HR, Sajda P (2014) Human scalp potentials reflect a mixture of decision-related signals during perceptual choices. *The Journal of Neuroscience* 34:16877–16889.

Plummer M (2003) JAGS: A program for analysis of Bayesian graphical models using Gibbs sampling In *Proceedings of the 3rd International Workshop on Distributed Statistical Computing (DSC 2003), Vienna, Austria.*

Pommier J, Renard Y (2005) Getfem++, an open source generic c++ library for finite element methods.

Ratcliff R (1978) A theory of memory retrieval. *Psychological Review* 85:59.

Ratcliff R, McKoon G (2008) The diffusion decision model: theory and data for two-choice decision tasks. *Neural Computation* 20:873–922.

Roitman JD, Shadlen MN (2002) Response of neurons in the lateral intraparietal area during a combined visual discrimination reaction time task. *Journal of neuroscience* 22:9475–9489.

Rouder JN, Morey RD (2012) Default bayes factors for model selection in regression. *Multivariate Behavioral Research* 47:877–903.

Schmolesky MT, Wang Y, Hanes DP, Thompson KG, Leutgeb S, Schall JD, Leventhal AG (1998) Signal timing across the macaque visual system. *Journal of neurophysiology* 79:3272–3278.

Schubert AL, Hagemann D, Frischkorn G (2017) Is intelligence little more than the speed of higher-order processing? *Journal of Experimental Psychology: General* .

Servant M, White C, Montagnini A, Burle B (2015) Using Covert Response Activation to Test Latent Assumptions of Formal Decision-Making Models in Humans. *Journal of Neuroscience* 35:10371–10385.

Servant M, White C, Montagnini A, Burle B (2016) Linking theoretical decision-making mechanisms in the simon task with electrophysiological data: A model-based neuroscience study in humans. *Journal of Cognitive Neuroscience* 28:1501–1521.

Shadlen MN, Kiani R (2013) Decision making as a window on cognition. *Neuron* 80:791–806.

Stanford TR, Shankar S, Massoglia DP, Costello MG, Salinas E (2010) Perceptual decision making in less than 30 milliseconds. *Nature neuroscience* 13:379–385.

Straube S, Grimsen C, Fahle M (2010) Electrophysiological correlates of figure–ground segregation directly reflect perceptual saliency. *Vision Research* 50:509–521.

Thorpe S, Fize D, Marlot C (1996) Speed of processing in the human visual system. *Nature* 381:520.

Tuerlinckx F (2004) The efficient computation of the cumulative distribution and probability density functions in the diffusion model. *Behavior Research Methods, Instruments, & Computers* 36:702–716.

Turner BM, Forstmann BU, Love BC, Palmeri TJ, Van Maanen L (2017) Approaches to analysis in model-based cognitive neuroscience. *Journal of Mathematical Psychology* 76:65–79.

Turner BM, van Maanen L, Forstmann BU (2015) Informing cognitive abstractions through neuroimaging: The neural drift diffusion model. *Psychological Review* 122:312–336.

van Vugt MK, Taatgen NA, Sackur J, Bastian M (2015) Modeling mind-wandering: a tool to better understand distraction In *Proceedings of the 13th International Conference on Cognitive Modeling*, pp. 252–257. University of Groningen.

Vandekerckhove J, Tuerlinckx F (2008) Diffusion model analysis with MATLAB: A DMAT primer. *Behavior Research Methods* 40:61–72.

Vandekerckhove J, Tuerlinckx F, Lee MD (2011) Hierarchical diffusion models for two-choice response times. *Psychological Methods* 16:44.

Verdinelli I, Wasserman L (1995) Computing Bayes factors using a generalization of the savage-dickey density ratio. *Journal of the American Statistical Association* 90:614–618 00422.

Vogel EK, Luck SJ (2000) The visual N1 component as an index of a discrimination process. *Psychophysiology* 37:190–203.

Voss A, Rothermund K, Voss J (2004) Interpreting the parameters of the diffusion model: An empirical validation. *Memory & Cognition* 32:1206–1220.

Wabersich D, Vandekerckhove J (2014) Extending JAGS: A tutorial on adding custom distributions to JAGS (with a diffusion model example). *Behavior Research Methods* 46:15–28.

Wagenmakers EJ (2009) Methodological and empirical developments for the Ratcliff diffusion model of response times and accuracy. *European Journal of Cognitive Psychology* 21:641–671.

Wagenmakers EJ, Lodewyckx T, Kuriyal H, Grasman R (2010) Bayesian hypothesis testing for psychologists: A tutorial on the savage–dickey method. *Cognitive psychology* 60:158–189.

Webster MA, De Valois RL et al. (1985) Relationship between spatial-frequency and orientation tuning of striate-cortex cells. *JOSA A* 2:1124–1132.

Zhang Q, van Vugt M, Borst JP, Anderson JR (2018) Mapping working memory retrieval in space and in time: A combined electroencephalography and electrocorticography approach. *NeuroImage* .

Zhang Q, Walsh MM, Anderson JR (2016) The effects of probe similarity on retrieval and comparison processes in associative recognition. *Journal of Cognitive Neuroscience* .

Figure Legends

Figure 1 Example stimuli of the *cue* and *response* intervals of medium noise conditions from Experiments 1 (top) and 2 (bottom). During the response interval, subjects decided which spatial-frequency-target each Gabor represented, pressing a button with their left hand for a low spatial frequency target (2.4 cycles per degree visual angle, cpd) and pressing a button with their right hand for a high spatial frequency target (2.6 cpd). N200 waveforms were calculated time-locked to the onset of the Gabor stimulus during the response intervals. In both experiments a paradigm was used in which the visual noise changed at 40 Hz and the Gabor signal flickered at 30 Hz to evoke 40 Hz and 30 Hz responses in electrocortical activity that track attention to the noise and signal stimuli. While the attention analysis is not discussed in this paper, a similar analysis is presented by Nunez et al. (2015).

Figure 2 A visual representation of the singular value decomposition (SVD) method for finding single-trial estimates

of evoked responses in EEG. The EEG presented here is time-locked to the signal onset during the response interval, such that the single-trial N200 waveform encoded the response to the signal onset. A single trial of EEG from one subject (Left) can be thought of as a time by channel ($T \times C$) matrix. SVD weights $\mathbf{v}$ ($C \times 1$) are obtained from the ERP response (i.e. trial-averaged EEG; $T \times C$) and can be plotted on a cartoon representation of the human scalp with intermediate interpolated values (Middle). This specific trial's N200 waveform (Right) was obtained by multiplying the time series data from each channel on this trial by the associated weight in vector $\mathbf{v}$ and then summing across all weighted channels. Weight averaging across channels is a common method to obtain larger signal-to-noise ratios in EEG (e.g. cleaner, more task-relevant neural signals, see Parra et al., 2005).

Figure 3 All trial-averaged N200 waveforms across EEG sessions and the six visual noise experimental conditions ($N = 147$). Smoothed histograms for the N200 deflection times (green distribution) as well as the N200 peak-latency times (blue distribution) are also displayed above. There was a significant but weak correlation found between the found N200 deflection times and the N200 peak-latency times ($\rho = .274$). N200 deflection times are not as variable across EEG sessions and noise conditions as N200 peak-latencies.

Figure 4 Left and right sagittal and posterior views of localized trial-averaged N200 waveforms averaged across all EEG recordings and noise conditions ($N = 147$). (Top) MNI scalp potential topographies (averaged projections of the first SVD components at the N200 peak-latency) were generated using spline-interpolation between electrodes. (Middle) Current Source Density MNI scalp topographies were generated with a Laplacian transform of the aforementioned data (Nunez and Pilgreen, 1991; Deng et al., 2012; Kayser and Tenke, 2015). (Bottom) The cortical maps were obtained by projecting the MNI-scalp spline-Laplacians onto one subject's anatomical fMRI image via Tikhonov (L2) regularization, maintaining similar distributions of activity of the surface Laplacians on the cortical surface. Blue and orange regions correspond to areas that produce negative and positive potentials observed on the scalp respectively.

Figure 5 Left: A scatter plot of trial-averaged N200 deflection times and 10th response time percentiles (an estimate of the processing time of time-invariant cognition across trials; NDT) Middle: A scatter plot of trial-averaged N200

peak-latencies and 10th response time percentiles. Observations were generated per noise condition and per EEG collection session ($N = 147$). Right: A scatter plot of single-trial N200 latencies versus single-trial response times. Observations were generated per trial ($N = 13{,}426$). Best-fit simple linear regression lines are shown in black with 95% confidence intervals for the intercept and slope parameters shown in gray. Overlaid on the linear regression lines are gold dashed lines representing the hypothesis with a slope of 1. That is, the expected influence of N200 peak-latency on response time is 1-to-1 millisecond if N200 peak-latency reflected human visual encoding time (VET).

Figure 6 Posterior distributions (Model 1) of effects of N200 peak-latency on non-decision time (NDT). Posterior distributions provide measures of parameter uncertainty in Bayesian model-fitting methods. If the posterior distributions had most of their density around the blue line, this would be strong evidence for the 1-to-1 relationship when the model assumptions are true. Posterior distributions with most of their density around the blue line would be evidence for the true effect equaling 1. Posterior distributions with most of their density around the red line would be strong evidence for the null hypothesis (the parameter equals 0). Some evidence exists for the effects of N200 peak-latency on NDT to be 1-to-1 (one millisecond increase in N200 peak-latency corresponds to a millisecond increase in NDT) as indicated by the Bayes Factors calculated with a Savage-Dickey density ratio (Verdinelli and Wasserman, 1995) of the posterior density over the prior distribution at $\gamma = 1$.

Figure 7 Posterior distributions (Model 2) of the *additional* effects (i.e. *moderator* effects) for each unique visual noise condition of N200 peak-latency on non-decision time (NDT). Posterior distributions provide measures of parameter uncertainty in Bayesian model-fitting methods. Posterior distributions with most of their density around the blue line would be evidence for the true effect equaling 1. Posterior distributions with most of their density around the red line would be strong evidence for the null hypothesis (the parameter equals 0). Evidence for the base effect of N200 peak-latency on NDT being 1-to-1 is similar to the results of Model 1 (top posterior distribution). The tests for moderator effects were inconclusive (all other posterior distributions). Not much evidence exists for moderator effects of condition. There is also not much evidence for *no* moderator effects as indicated by the Bayes Factors for the null effects BF near 1.

Figure 8 The addition of more trials from contaminant processes resulted in some non-decision time (NDT) estimates being negatively biased towards smaller values. This, in turn, resulted in decreased linear relationships (e.g. less than 1-to-1) between true NDT and estimated NDT. This was especially true for the estimates of simple drift-diffusion (DDM) model parameters. This simulation suggested that while 10th response time percentiles were positively biased as estimates of true NDT (e.g. true NDT were approximately 60 ms shorter than the 10th response time percentiles), the 1-to-1 relationship could be well estimated by the 10th percentiles but not the DDM fitting procedure when there were greater than 1% of trials with an unremoved contaminant process. This fact explains why a true measure of VET, such as the proposed N200 peak-latency, might not track DDM-estimated NDT as well as the 10th response time percentiles.

Figure 9 A graphical illustration of a Neural Drift Diffusion model in which the visual encoding time τ_e on single-trials describes the latency of the negative peaks of the N200 waveform on 146 experimental trials. Single-trial observations of the N200 peak-latency are found by using a decomposition of the average ERP response at each electrode and then biasing the raw EEG by the resulting channel weights. Total NDT τ reflects both visual encoding time (VET) τ_e as well as residual motor response τ_m (e.g. motor execution time after the decision is made) and can be estimated from response time distributions. Decision time is generated via a Brownian motion evidence accumulation process with evidence accumulation rate δ (drift rate), evidence accumulation noise ς (diffusion coefficient), and evidence threshold (boundary parameter) α (for more information see Ratcliff, 1978; Ratcliff and McKoon, 2008; Nunez et al., 2015, 2017)